Redox Biology 85 (2025) 103769

Contents lists available at ScienceDirect

Redox Biology

journal homepage: www.elsevier.com/locate/redox

Enhancing protein O-GlcNAcylation in down syndrome mice mitigates memory dysfunctions through the rescue of mitochondrial bioenergetics, stress responses and pathological markers

Chiara Lanzillotta [a], Francesca Prestia [a], Viviana Greco [b,c], Federica Iavarone [b,c], Federica Cordella [d,e], Chiara Sette [a], Elena Forte [a], Antonella Tramutola [a], Simona Lanzillotta [a], Tommaso Cassano [f], Silvia Di Angelantonio [d,e,g], Andrea Urbani [b,c], Eugenio Barone [a], Marzia Perluigi [a], Fabio Di Domenico [a,*]

[a] Department of Biochemical Sciences A. Rossi Fanelli, Sapienza University of Rome, Piazzale Aldo Moro 5, 00185, Rome, Italy
[b] Department of Basic Biotechnological Sciences, Intensivological and Perioperative Clinics, Università Cattolica del Sacro Cuore, 00168, Rome, Italy
[c] Department of Laboratory Diagnostic and Infectious Diseases, Unity of Chemistry, Biochemistry and Clinical Molecular Biology, Fondazione Policlinico Universitario Agostino Gemelli-IRCCS, 00168, Rome, Italy
[d] Center for Life Nano- & Neuroscience, Istituto Italiano di Tecnologia, Viale Regina Elena, 291, 00161, Rome, Italy
[e] Department of Physiology and Pharmacology, Sapienza University of Rome, Piazzale Aldo Moro 5, 00185, Rome, Italy
[f] Department of Medical and Surgical Sciences, University of Foggia, Via Luigi Pinto, c/o Policlinico "Riuniti" di Foggia, 71122, Foggia, Italy
[g] D-Tails srl BC, Via di Torre Rossa, 66, 00165, Rome, Italy

ARTICLE INFO

Keywords:
O-GlcNAc
Down syndrome
OGA
OGT
APP
Tau
Proteomics

ABSTRACT

Disturbances of the single sugar modification of proteins, O-GlcNAc, have been identified as a potential connection between disrupted brain metabolism and intellectual decay. In Alzheimer disease (AD), the reduced uptake of glucose in the brain results in aberrant O-GlcNAc cycling contributing to redox imbalance and neurodegeneration. Notably, alterations of O-GlcNAc homeostasis, associated with impaired O-GlcNAc transferase (OGT)/O-GlcNAcase (OGA) regulation, foster neuropathological mechanisms characterized by the presence of AD hallmarks in Down syndrome (DS) models. In the present study we examined the ability of Thiamet G (TMG), a well-known OGA inhibitor, in improving bio-energetic processes, inducing stress responses, reducing AD-related signatures and ameliorating cognition in a murine model of DS. Our data demonstrate that short-term intranasal administration of TMG restored OGA activity and normalized the global O-GlcNAc profile in mouse cortices. By a proteomic approach we identified protein components whose increased O-GlcNAc levels rescue, resulted to brain molecular and cognitive improvements. Remarkably, these included elements involved in energy production, neuronal architecture, antioxidant and stress response mechanisms. The ability of TMG in rescuing O-GlcNAc cycle and metabolic changes, associated with improved mitochondrial activity in cortical tissue, was further accompanied by changes in the O-GlcNAc/phospho ratio of APP and Tau. Functional improvements translated in enhanced recognition memory in Ts2Cje mice. Our study highlights the pivotal role of altered protein O-GlcNAcylation in DS neuropathology and establishes the molecular basis to envision the O-GlcNAc process as a promising therapeutic target to mitigate genetic- and metabolism-driven brain alterations linked to redox imbalance, mitochondrial failure and the development of AD features.

1. Introduction

Compelling evidence suggests that the disruption of protein O-GlcNAc modification (O-GlcNAcylation) represents a molecular relationship between disturbed brain metabolism and intellectual disabilities [1–4]. O-GlcNAcylation is a non-canonical form of glycosylation characterized by the attachment of a single O-linked N-acetylglucosamine (O-GlcNAc) residue to nuclear and cytoplasmic proteins [5]. This reversible and dynamic PTM is tightly regulated by the opposing enzymatic activities of O-GlcNAc transferase (OGT) and

* Corresponding author. Department of Biochemical Sciences A. Rossi Fanelli, Sapienza University of Rome, P.le Aldo Moro 5, 00185, Rome, Italy.
E-mail address: fabio.didomenico@uniroma1.it (F. Di Domenico).

https://doi.org/10.1016/j.redox.2025.103769
Received 15 May 2025; Received in revised form 24 June 2025; Accepted 14 July 2025
Available online 16 July 2025

O-GlcNAcase (OGA), ensuring a delicate balance [6,7]. Furthermore, the O-GlcNAc modification is strictly reliant on the availability of uridine diphosphate N-acetylglucosamine (UDP-GlcNAc) synthesized by the hexosamine biosynthetic pathway, a branch of glycolysis [8,9]. Notably, O-GlcNAcylation occurs primarily on serine (S) and threonine (T) residues, allowing it to compete with phosphorylation at the same or nearby sites. This adds a supplementary layer of regulatory complexity to various signalling processes and transcriptional factors in response to nutrient availability or endogenous stimuli [10–12]. Aberrant protein O-GlcNAc modification levels, resulting from brain energy failure, have been observed in Alzheimer's disease (AD). These changes have been associated with the accumulation of pathological hallmarks, synaptic dysfunction, disrupted neuronal signalling, mitochondrial failure and redox imbalance [13–17]. In addition, recent reports from our laboratory have recognized a role for altered O-GlcNAc modification in the progression of Down syndrome (DS) neuropathology [18]. Individuals with DS are characterized by the presence of the triplication of Chromosome 21 (HSA21), which leads to the early onset (by the age of 40) of AD-like pathology. DS brain shows the early buildup of β-amyloid (Aβ) plaques and neurofibrillary tangles (NFTs) in the cerebral cortex, which subsequently spread to the hippocampus, striatum, and cerebellum [19,20]. The increased accumulation of Aβ is directly attributed to the triplication of the amyloid precursor protein *(APP)* gene located on HSA21 [21]. The overexpression of specific kinases, such as DYRK1, which interact with Tau but also with APP, draws further connections between genetic imbalances and neuro-pathological phenotypes [22,23]. Additional mechanisms of neurodegeneration shared by both DS and AD, include brain hypoglycemia, insulin resistance, dysfunction of oxidative phosphorylation (OXPHOS) and increased levels of oxidative stress (OS). The latter aspect is associated with triplication of genes regulating redox responses (e.g. *SOD1; BACH1*) [24–27]. These findings indicate that DS may represent a valuable preclinical model for investigating AD-related neuropathology and cognitive decline. However, understanding the molecular processes connecting genetic abnormalities and metabolic dysfunctions to brain alterations and reduced cognition remains an ongoing area of investigation. We recently demonstrated, in a mouse model of DS, the reduction of protein O-GlcNAcylation levels resulting from a combination of disrupted OGT/OGA cycling and AMPK-associated inhibition of GFAT1, the rate-limiting enzyme of the hexosamine biosynthetic pathway (HBP) [17,28,29]. These alterations likely reflect the complex interplay between gene dosage imbalance and metabolic stress in initiating the neurodegenerative cascade [18], although the underlying molecular processes require further investigation. Within this context, delving into mechanistic analysis of O-GlcNAc role in DS neuropathology, with the intent of evaluating OGA enzyme activity as a potential therapeutic target to enhance cognitive function, might offer valuable advancement in the field.

In the present study, we treated the transgenic murine model of DS, Ts2Cje (Ts2) [30], with Thiamet G (TMG), a potent OGA inhibitor, to corroborate and further explore its beneficial effects in mitigating AD signatures and cognitive impairments. By using a 2-DE proteomics approach, we identified specific protein components whose pharmacological rescue, in terms of O-GlcNAc levels, contributes to improvements in brain molecular dynamics. Remarkably, re-tuning O-GlcNAcylation across crucial components involved in metabolic, redox and stress response pathways ameliorated mitochondrial defects and improved bioenergetics pathways. Our data strongly emphasize the need to preserve O-GlcNAc homeostasis in the brain, but also support the value of TMG administration in retuning O-GlcNAc cycling to reduce neurodegenerative outcomes associated with AD.

2. Materials and methods

2.1. Animal model

Experiments were carried out on 6-month-old Ts2Cje (Ts2) mice (Rb(12.Ts171665Dn)2Cje) and age-matched euploid (Eu) controls (B6EiC3SnF1). The Ts2 mouse harbours a trisomic Robertsonian fusion chromosome that includes distal regions of mouse chromosomes MMU16 and MMU12. Breeding pairs were obtained from Jackson Laboratories (Bar Harbor, ME, USA), and the colony was maintained by repeatedly crossing Ts2 trisomic females with euploid males. Genotyping of the progeny was performed via quantitative PCR to identify the presence of the trisomic segment, as described by Reinholdt et al. [31]. Mice were housed in clear Plexiglas cages (20 × 22 × 20 cm) under standard laboratory conditions (22 ± 2 °C, 70 % humidity, 12-h light/dark cycle) with ad libitum access to food and water. All procedures strictly adhered to Italian national legislation (DL 116/92) and the European Communities Council Directive (86/609/EEC). Experimental protocols were approved by the Italian Ministry of Health (#522/2020-PR and #426/2024-PR). Efforts were made to minimize animal use and suffering. All biological samples were immediately flash-frozen and stored at −80 °C until further use.

2.2. Thiamet-G intranasal treatment

TMG is a highly potent and selective inhibitor of O-GlcNAcase (OGA) and is currently the most widely utilized compound for OGA inhibition [13]. TMG demonstrates excellent inhibitory efficacy (Ki = 21 nM) and good selectivity, however a few studies demonstrated off-target effects, including overactivation of GSK-3β and potential interference with other enzymes like β-hexosaminidase, when used at high doses or administrated to the brain [32]. Previous work from our laboratory demonstrated that intranasal (IN) delivery of 25 μg TMG significantly elevated total protein O-GlcNAc levels in murine hippocampus [18]. Our intranasal delivery protocol enabled direct brain targeting, allowing for a reduced TMG dose and thereby potentially minimizing side effects or off-target effects, while still maintaining stable OGA inhibition. In this study, 6-month-old Ts2 and Eu mice were assigned to one of four experimental groups based on genotype and treatment: vehicle (PBS 1X, Veh) or TMG (25 μg; HY-12588, MedChemExpress). The groups included: Eu Veh, Eu TMG, Ts2 Veh, and Ts2 TMG. Mice received 10 μL per nostril of either Veh or TMG, administered twice a day for five consecutive days. Supplementary Table 1 details the number of animals used (6/7 per group), their sex (Male/Female: 3/3 or 4/3), average age (≈6.7 months), and both initial and final weights. The TMG regimen was well tolerated, with only a minor, non-significant weight loss observed across all groups. No alterations in food or water intake were detected. Following the treatment period, mice were subjected to behavioural assessments. Subsequently, mice were euthanized and perfused intracardially with sterile PBS. Brain regions were then collected and preserved for subsequent biochemical and molecular analyses.

2.3. Behavioral tasks

The Novel Object Recognition (NOR) test is commonly employed to evaluate cognitive function, particularly recognition memory, in rodent models of neurodegeneration. The NOR paradigm exploits rodents' innate tendency to explore novel objects over familiar ones. The procedure consists of three periods: habituation, familiarization, and test. During the habituation (Day 1), animals are free to explore an open-field arena (50 cm × 30 cm × 30 cm) for 10 min without any objects. On Day 2 (familiarization), each mouse is placed in the arena with two identical objects for 10 min. To avoid bias, animals are introduced facing away from the objects. During the test, conducted 24 h later, one of the familiar objects is replaced with a novel one and exploration behaviour is recorded [33,34]. Cognitive performance is assessed using the

discrimination index (DI = [TN − TF]/[TN + TF]), reflecting the ability to distinguish between novel (TN) and familiar (TF) objects. The preference index (PI) is calculated as the time spent exploring a specific object divided by the total exploration time, expressed as a percentage: PI = [C/(A, B + C)] × 100. A PI above 50 % indicates novel object preference, below 50 % indicates familiar object preference, and 50 % indicates no preference.

The Y-maze test was conducted to assess spatial memory and exploratory activity, as previously described [35]. The Y-maze apparatus comprises three arms (A, B, and C), each 40 cm long, forming a Y-shape at 120° angles, converging in a central triangular zone. The test includes two phases: (i) a training session, where one arm is blocked and the mouse explores the remaining arms, and (ii) a testing session following a 30-min inter-trial interval, during which all three arms are accessible. Spatial memory is evaluated based on the time spent exploring the previously blocked, now novel arm (NA), calculated as: time in novel arm/total time in all arms × 100 (%).

2.4. Immunofluorescence

Brain hemispheres were fixed in 4 % formaldehyde at 4 °C for 24 h. Following fixation, the brains were cryoprotected for 48 h at 4 °C in a solution containing 20 % sucrose and 0.02 % sodium azide (NaN_3). The hemispheres were then frozen using a temperature-controlled freezing stage, coronally sectioned at 20 μm with a sliding cryostat (Leica Biosystems, Wetzlar, Germany), and stored in Phosphate Buffered Saline (PBS; PPB006, Sigma-Aldrich). Sections were mounted on glass slides and, once dried, subjected to heat-induced antigen retrieval in 10 mM EDTA (pH 6.0) at 55 °C for 20 min. After four washes in filtered PBS, sections were blocked with 10 % normal goat serum and 0.2 % Triton X-100 in PBS. Slides were then incubated overnight at 4 °C with the following primary antibodies: anti-*O*-GlcNAc CTD110.6 (1:100; mouse, SC-59623, Santa Cruz Biotechnology), anti-*O*-GlcNAc RL2 (1:50; mouse, MABS157, Sigma-Aldrich), anti-Tau S202/Y205 [AH36] (1:500; rabbit, SMC-601, StressMarq Biosciences), and anti-pAPP T668 (1:500; rabbit, PA5-97328, Invitrogen Thermo Fisher Scientific). After washing with PBS, sections were incubated for 2 h at room temperature with Alexa Fluor 488- and 647-conjugated secondary antibodies (1:1000; A11029, A32733, Invitrogen Thermo Fisher Scientific). To reduce tissue autofluorescence, sections were stained with 0.1 % Sudan Black B in 70 % ethanol (199664, Sigma-Aldrich), followed by incubation with DAPI (10 mg/mL; IS-7712, Immunological Sciences) for 5 min. After final washes, coverslips were mounted using Fluoromount aqueous medium (F4680, Sigma-Aldrich) and left to dry at room temperature. Negative controls omitting primary antibodies were included to assess nonspecific background staining.

2.5. Image acquisition, threshold analysis and colocalization

Images were obtained using an Olympus IX73 inverted microscope equipped with the X-Light V3 Spinning Disk Confocal module (Crest Optics), LDI laser source, and a Prime BSI Scientific CMOS (sCMOS) camera with 6.5 μm pixels (Photometrics). A 60x/NA 1.35 oil immersion objective (Olympus) was used, capturing images in z-stack mode with a z-step of 0.2 μm. Image acquisition was controlled using Metamorph software version 7.10.2 (Molecular Devices, Wokingham, UK). Quantification of AT8, APP, and glycosylation signals was conducted using Fiji software, measuring fluorescence intensity within the field of view (FOV). Z-stack images were processed into maximum intensity z-projections, followed by background noise removal and image binarization. Fluorescence thresholds were adjusted to accurately identify marker-positive cells. Colocalization analysis between AT8/O-GlcNAc and APP T668/O-GlcNAc was performed using the "JaCOP" plugin of Fiji software. Specifically, channels 1 and 2 corresponding to the selected signals were chosen for analysis, and masks were applied to AT8 and APP signals to quantify the extent of colocalization with O-GlcNAcylation signals.

2.6. Subcellular fractionation

Subcellular fractionation was performed on frontal cortex of Ts2 mice (treated with Veh and TMG). All steps for subcellular fractionation were performed following the protocol described by Dimauro et al. [36] optimized for brain tissues. The purity of the fractions was validated by assessing Histone H3 in nuclear fractions and the Complex I subunit (NDUFB8) in mitochondrial fractions by Western Blotting (WB). (Supplementary Fig. 1).

2.7. RNA extraction and quantification RT-PCR

RNA was extracted from the frozen cortex of Eu Veh, Eu TMG, Ts2 Veh, and Ts2 TMG using Tissue Total RNA Kit according to the manufacturer's instructions (Abcam). RNA was quantified using the SpectraMaxi3x (Molecular Devices) and cDNA was reverse transcribed using the cDNA High-Capacity kit (Applied Biosystems, Foster City CA). The standardized samples were added to the High-Capacity RNA-to-cDNA kit (Applied Biosystems, Foster City, CA) including reverse transcriptase, random primers, dNTPs and buffer according to the manufacturer's instructions. The cDNA was produced through a series of heating and annealing cycles in the MultiGene OPTIMAX 96-well Thermocycler (LabNet International, Edison, NJ, USA). Real time PCR was carried out using the CFX OPUS96 (Bio-Rad Laboratories) and considering the following cycling conditions: 35 cycles of denaturation at 95 °C for 20 s; annealing and extension at 60 °C for 20 s, using the SensiFAST™ SYBR® No-ROX Kit (Bioline, London, UK). 1 μl of cDNA (100 ng/ul of standardized RNA samples) was diluted with 7 μl of RNAse-free water, 10 μl of SensiFAST SYBR® No-ROX Mix. Gene expression was evaluated by normalizing to B2M expression as an internal control. Fold change was determined using the 2–ΔΔCt method [37]. Primers used for the evaluation of the gene expression are reported in Supplementary Table 2.

2.8. Western blot

Frontal cortex samples were lysed in RIPA buffer (pH 7.4) containing 50 mM Tris-HCl, 150 mM NaCl, 1 % NP-40, 0.25 % sodium deoxycholate, 1 mM EDTA, 0.1 % SDS, protease inhibitor cocktail (1:100; 539132, Millipore), phosphatase inhibitor cocktail (1:100; P5726, Sigma-Aldrich), PUGNAc (OGA inhibitor, 100 μM; A7229, Sigma-Aldrich), and Benzyl-2-Acetamido-2-Galactopyranose (OGT inhibitor, 2 mM; B4894, Sigma-Aldrich). The tissue underwent sonication and centrifugation for 30 min at 14,000 rpm and 4 °C. The supernatant was collected to determine protein concentration using the BCA method (Pierce™ BCA Protein Assay Kit, 23227, Thermo Fisher Scientific) according to the manufacturer's instructions. Subsequently, 15 μg of proteins were separated by SDS-PAGE using Criterion™ TGX Stain-Free™ precast gels (Bio-Rad) and transferred to a nitrocellulose membrane via the Trans-Blot Turbo Transfer System (Bio-Rad). Images were taken by the ChemiDoc MP imaging system (Bio-Rad) with Stain-Free blot settings, and total protein load was normalized based on Stain-Free technology. Membranes were incubated with 3 % BSA (9048-46-8, SERVA) or 5 % milk (skim milk powder; 42590, SERVA) in 1X Tris-buffered saline (TBS; #1706435, Bio-Rad) containing 0.01 % Tween20 and incubated overnight at 4 °C with the following primary antibodies: OGA (1:1000; SAB-4200267, Sigma-Aldrich), O-GlcNAc CTD110.6 (1:500; SC-59623, Santa Cruz Biotechnology), O-GlcNAc RL2 (1:1000; MABS157, Sigma-Aldrich), OGT (1:500; SC-74546, Santa Cruz Biotechnology), pS/T (1:5000; ab17464, Abcam), pTau T181 (1:1000; 701530, Invitrogen Thermo Fisher Scientific), p-APP T668 (1:1000; PA5-97328, Invitrogen Thermo Fisher Scientific), AT8 (1:1000; MN1020, Invitrogen Thermo Fisher Scientific), APP (1:5000; SAB5200113, Sigma-Aldrich), OXPHOS (1:2000; ab110413, Abcam), NDUFB8 (1:1000; NBP2-75586, Novus Biologicals), NRF2 (1:1000;

GTX103322, Gene Tex), BACH1 (1:500; orb4401; Biorbyt), ATF4 (1:500, SC-390063, Santa Cruz Biotechnology), HO-1 (1:1000, ADI-SPA-895-F, Enzo Life Sciences), NQO1 (1:1000, 15926, Invitrogen Thermo Fisher Scientific), pAMPK T172 (1:1000; GTX52341, GeneTex), AMPKα1/2 (1:500; SC-74461, Santa Cruz Biotechnology), pGFAT1 S243 (1:1000; S343C, MRC-PPU), GFAT1 (1:1000; 28121, IBL), PGC1α (1:1000; SC-13067, Santa Cruz Biotechnology), TFAM (1:500; SC-166965, Santa Cruz Biotechnology), and Histone H3 (1:1000, #9715, Cell Signaling). The following day, membranes were washed with 1X TBS containing 0.01 % Tween20 (T-TBS) and incubated for 1 h at room temperature with the appropriate horseradish peroxidase-conjugated secondary antibodies: anti-rabbit (1:10,000; L005661, Bio-Rad), anti-mouse (1:10,000; L005662, Bio-Rad). Blots were imaged using the ChemiDoc MP imaging system with chemiluminescence settings. Relative protein abundance was calculated using total protein normalization and analyzed with Image Lab 6.1 software (Bio-Rad).

2.9. Slot blot analysis

Protein-bound 3-nitrotyrosine (3-NT) and protein carbonyl (PC) levels were evaluated using cortical homogenates. For 3-NT, 3 μL of homogenate was incubated with 6 μL Laemmli buffer (0.125 M Tris, 4 % SDS, 20 % glycerol) for 20 min at room temperature. For PC, 3 μL of homogenate was derivatized with 10 mM DNPH and 5 μL of 12 % SDS for 20 min, followed by neutralization with 7.5 μL of 2 M Tris in 30 % glycerol. Protein samples for both assays were loaded onto nitrocellulose membranes using a slot blot apparatus under vacuum. The membranes were blocked for 1 h at room temperature with 3 % BSA in TBS containing 0.01 % Tween 20, then incubated with primary antibody (anti-3-NT, 1:500; MAB3248, Bio-techne R&D Systems) for 2 h at room temperature. After washing, membranes were incubated with alkaline phosphatase-conjugated secondary antibody for 1 h, washed, and developed with BCIP/NBT substrate. Images were captured using the ChemiDoc MP system (Bio-Rad) and analyzed with Image Lab 6.1 software (Bio-Rad).

2.10. OGA assay

OGA enzymatic activity was evaluated using the artificial substrate *p*-nitrophenyl N-acetyl-β-D-glucosaminide (pNP-GlcNAc), following the protocol outlined by Zachara et al. [38]. In brief, 15 mg of frozen frontal cortex tissue was lysed in RIPA buffer (pH 7.4) containing 50 mM Tris, 50 mM NaCl, 1 % NP-40, 0.25 % sodium deoxycholate, 1 mM EDTA, 0.1 % SDS, and supplemented with protease (1:100; 539132, Millipore) and phosphatase (1:100; P5726, Sigma-Aldrich) inhibitor cocktails. The sample was homogenized using 20 strokes with a Wheaton tissue grinder, followed by sonication and centrifugation at 14,000 rpm for 40 min at 4 °C to clear insoluble material. The resulting supernatant was desalted using Zeba™ Spin Desalting Columns (89882, Thermo-Fisher Scientific), and protein content was quantified via the BCA assay. For the enzymatic assay, 150 μg of total protein was incubated at 37 °C for 2 h in a reaction buffer consisting of 2 mM pNP-GlcNAc, 50 mM sodium cacodylate (pH 6.4), 50 mM N-acetylgalactosamine, and 0.3 % BSA. The reaction was terminated by the addition of 500 mM Na_2CO_3, and absorbance was read at 405 nm using a Multiskan EX spectrophotometer (Thermo Lab systems). OGA activity was calculated based on the release of *p*-nitrophenol (pNP), with one unit defined as the amount of enzyme releasing 1 μmol of pNP per minute. Activity levels were normalized against total protein expression for each sample group.

2.11. Elisa analysis of Aβ 1–42 peptide

Amyloid β 1–42 peptide levels were quantified using the Mouse Aβ 1–42 ELISA Kit (KMB3441; Invitrogen, Thermo Fisher Scientific) in Ts2 and Eu mice treated with either Veh or TMG, with six animals per group. For sample preparation, ~10 mg of cortical tissue was homogenized in ice-cold diethanolamine (DEA) buffer (10 μl/mg tissue), composed of 0.2 % DEA in 50 mM NaCl and supplemented with a protease inhibitor cocktail (1:100; 539132, Millipore). Samples were then centrifuged at 15,000 rpm for 90 min at 4 °C, and the resulting supernatant was collected as the soluble Aβ fraction. Quantification of Aβ1-42 was carried out according to the manufacturer's instructions. Data analysis and curve fitting were performed using GraphPad Prism version 10.4 (GraphPad Software, La Jolla, CA, USA).

2.12. Respiratory chain complexes activity and ATP content

Respiratory chain complex activities and ATP levels were assessed in cryopreserved frontal cortex samples from Eu and Ts2 mice treated with either Veh or TMG. Tissue cryopreservation followed the method outlined by Valenti et al. [39]. High-resolution polarographic measurement of oxygen consumption was conducted using a NextGen-O2k oxygraph (OROBOROS Instruments, Austria) equipped with a 1.5 mL chamber and a Clark-type oxygen electrode. Assays were performed at 37 °C with constant stirring at 750 rpm in respiration buffer containing 3 mM $MgCl_2$, 20 mM taurine, 10 mM KH_2PO_4, 20 mM HEPES, 110 mM sucrose, 0.1 % BSA, and 5.5 mM glucose. Oxygen flux (JO_2), representing the rate of oxygen consumption, was continuously recorded at 1-s intervals using DatLab software under phosphorylating conditions with saturating levels of ADP. Sequential additions to the chamber were made to assess individual complex activities: 10 mM glutamate and 2 mM malate to initiate Complex I activity, followed by 5 mM ADP; 5 mM succinate to activate Complex II; 0.5 μM rotenone to inhibit Complex I; 2.5 μM antimycin A to block Complex II; and finally, 2 mM ascorbate with 0.8 mM TMPD to drive Complex IV activity, which was subsequently inhibited with 2 mM sodium cyanide (NaCN).

2.13. Two-dimensional electrophoresis (2-DE) gels and blots

For first-dimension electrophoresis, 100 μg of protein (in ~200 μL volume) from 6-month-old Ts2 mice treated with Veh or TMG was loaded onto 110-mm pH 3–10 Immobilized pH Gradient (IPG) Ready Strips (Bio-Rad). The strips underwent active rehydration in a Protean IEF cell (Bio-Rad) at 50 V for 18 h. Isoelectric focusing was carried out using a stepwise voltage protocol: 300 V for 1 h, a linear increase to 8000 V over 5 h, and then continued focusing to reach a total of 20,000 V/h. IPG strips were stored at −80 °C until further processing.

For the second dimension, strips were thawed and equilibrated in 50 mM Tris-HCl buffer (pH 6.8) containing 6 M urea, 1 % SDS, 30 % glycerol, and 0.5 % dithiothreitol for 10 min, followed by re-equilibration in the same buffer with 4.5 % iodoacetamide replacing dithiothreitol for 15 min. SDS-PAGE was performed on 12 % linear gradient Criterion Bis-Tris gels (Bio-Rad) at 200 V for 50 min. Protein standards (Precision Plus, Bio-Rad) were included for molecular weight reference. Following electrophoresis, gels were fixed in 10 % acetic acid and 40 % methanol for 40 min and stained overnight with SYPRO Ruby (Bio-Rad) at room temperature. Excess stain was removed, and gels were stored in deionized water. For two-dimensional immunoblotting, proteins were transferred to nitrocellulose membranes (Bio-Rad). Membranes were blocked with 3 % BSA in T-TBS for 1 h and incubated overnight at 4 °C with a cocktail of primary antibodies against O-GlcNAc: CTD110.6 (1:500; Santa Cruz Biotechnology) and RL2 (1:1000; Sigma-Aldrich). After three washes in T-TBS (10 min each), membranes were probed with alkaline phosphatase-conjugated anti-mouse IgG secondary antibody (1:5000; Sigma-Aldrich) for 1 h at room temperature. Signal detection was performed using BCIP/NBT substrate.

2.14. Image analysis and in-gel trypsin digestion/peptide extraction

Gel and blot images stained with SYPRO Ruby were captured using a Chemidoc MP System (Bio-Rad) and saved in TIFF format. A total of 12 gels and 12 blots were analyzed using PD-Quest 2D Analysis software

(v7.2.0; Bio-Rad). The PD-Quest spot-detection tool facilitated the comparison of 2D gels and blots from Ts2 Veh and Ts2 TMG samples. A master gel was first selected, and all gels and blots were normalized based on total spot density. The gel-to-blot comparison process involved two steps: manual identification of common spots across the gels and blots, followed by automated matching based on user-defined parameters for spot detection, including both faint and large spots. This procedure generated a dataset containing 400–800 spots, with only proteins exhibiting significant differential expression between groups being considered for identification. To quantify these differences, analysis sets were created using PD-Quest's analysis set manager, and pixel counts corresponding to protein level changes were calculated. Image analysis was conducted on both blots and SYPRO Ruby-stained gels, with glycosylation data normalized to expression levels. Proteins showing significant changes between Ts2 Veh and Ts2 TMG were excised from the gels and placed in individual Eppendorf tubes for trypsin digestion according to established protocols [17]. The resulting tryptic peptides were stored at −80 °C for MS/MS analysis.

2.15. RP-HPLC-high resolution MS/MS characterization of tryptic peptides and MS data analysis

Tryptic peptide analysis was performed using the UltiMate™ 3000 RSLC-nano System connected to an Orbitrap Fusion Lumos Tribrid Mass Spectrometer and EASY-Spray nanoESI (Thermo Fisher Scientific, Waltham, MA, USA). Chromatographic separation was carried out on an EASY-Spray PepMap C18 column (15 cm long, 50 μm internal diameter (ID), 2 μm particles, 100 Å pore size) (Thermo Fisher Scientific), coupled with an Acclaim PepMap100 nano-trap cartridge (C18, 5 μm, 100 Å, 300 μm ID x 5 mm) (Thermo Fisher Scientific). Separation was done at 40 °C using a gradient elution, with a mobile phase flow rate of 0.3 μL/min. The eluent A was an aqueous formic acid (FA) solution (0.1 %, v/v), and eluent B was an ACN/FA solution (99.9:0.1, v/v), with the following gradient: (i) 5 % B for 7 min, (ii) from 5 % to 55 % B over 35 min, (iii) from 55 % to 90 % B over 3 min, (iv) 90 % B for 5 min, (v) from 90 % to 5 % B over 2 min, (vi) 5 % B for 7 min, resulting in a total run time of 65 min. The injection volume was 5 μL. LC-MS was conducted in positive ionization mode with a resolution of 120,000 in the 150–2000 m/z acquisition range. MS/MS fragmentation was achieved by collision-induced dissociation (HCD, 30 % normalized collision energy) in Data-Dependent Scan (DDS) mode. The minimum signal was set to 500.0, the isolation width to 2 m/z, and the default charge state to +2. MS/MS spectra were acquired using the Orbitrap mass analyzer. Tuning parameters included a capillary temperature of 275 °C and a source voltage of 4.0 kV. The MS/MS data were processed using Proteome Discoverer 2.4.1.15 (Thermo Fisher Scientific), based on the SEQUEST HT algorithm (University of Washington, USA, licensed to Thermo Electron Corp., San Jose, CA, USA) and SEQUEST HT cluster as the search engine against the Mus musculus database (UniProtKB/Swiss-Prot Knowledge database; 17,834 entries). The search parameters included a 10 ppm tolerance for precursor ions and 0.5 Da for-product ions, allowing for up to 2 missed cleavages. Carbamidomethylation of cysteine (+57.02 Da) was set as a fixed modification, while oxidation of methionine (+15.99 Da) and O-GlcNAc (+203.1950 Da) were considered as variable modifications on Serine and Threonine. Protein identification was based on a minimum of two peptides per protein and two unique peptides, with a high confidence filter applied.

2.16. Protein ontologies, networks and statistical analysis

To identify biologically relevant molecular pathways, proteomic datasets were analyzed using a variety of bioinformatics tools and databases, including QIAGEN's Ingenuity Pathway Analysis (IPA, Version 01-22-01, QIAGEN, Aarhus, DK), the UNIPROT database (https://www.uniprot.org), PANTHER software (https://www.pantherdb.org), STRING software (https://string-db.org) and REACTOME database (https://reactome.org) [40,41]. These platforms were used to explore functional associations pertinent to the experimental findings. Analysis parameters included both direct and indirect interactions, incorporating endogenous chemical substances, with a summary filter considering all molecules and relationships. The most significant pathways, categories, diseases, and functions linked to the datasets were identified by calculating their significance (p-value, Fisher's exact test). A p-value threshold of 0.05 was applied to assess the probability of association between genes/proteins in the datasets and each pathway or function (including canonical pathways and biological functions).

Statistical analyses of immunofluorescence and immunochemical data were performed using the Student's t-test for comparisons between two groups and a non-parametric one-way ANOVA followed by a post-hoc Fisher LSD test for comparisons involving more than two groups. Data are presented as mean ± SEM for each group. GraphPad Prism 10.4 (GraphPad, La Jolla, CA, USA) was used for data analysis and plotting.

3. Results

3.1. Intranasal TMG administration reduces OGA activity and increases total O-GlcNAc levels in the frontal cortex of Ts2 mice

6-month-old Ts2 and age-matched Eu were administered either with Veh solution or 25 μg of TMG by intranasal route (Fig. 1A) aiming to target the brain and avoid side-effects to peripheral organs [42]. The choice of a short-term administration protocol aimed to identify early modifications at the expenses of molecular mechanisms modulated by acute TMG delivery and assess their potential effects on mice cognition. Additionally, we confirm that TMG administration does not produce any detectable toxicity, consistent with previous reports and with recent phase I clinical trials [43]. After 5 days of treatment, we examined the biochemical impact of TMG in the frontal cortex of Ts2 mice, by evaluating total O-GlcNAc levels (RL2+CTD110.6 antibodies were employed) and OGA/OGT cycling. The analysis of total O-GlcNAc levels revealed a reduction in Ts2 mice compared to the Eu Veh group (−33 %, $p = 0.04$) (Fig. 1B and D). TMG treatment efficiently increased the levels of O-GlcNAcylated proteins in both Eu (+70 % vs. Eu Veh, $p = 0.0008$) and Ts2 mice (+79 % vs. Ts2 Veh, $p = 0.0001$) (Fig. 1D). Subsequently, we analyzed total protein phosphorylation on S and T residues (pS/T) showing a decrease in Ts2 mice following TMG treatment (−65 % vs. Ts2 Veh, $p = 0.0008$, Fig. 1C and E). This analysis delineates an inverse relationship between O-GlcNAc and pS/T in Ts2 mice, which is successfully reversed by TMG treatment (Fig. 1H). The improvement of O-GlcNAc was further confirmed by confocal microscopy analyses that show an increase for Covered area % in Ts2 TMG vs. Veh mice (+3.7, $p < 0.0001$) (Fig. 1F and G). In agreement with previous data [18], the reduction of O-GlcNAc observed in Ts2 mice is driven by increased OGA protein levels in Ts2 (+134 %, $p = 0.04$, Fig. 2A and B). Rather, the administration of TMG inhibits OGA enzyme activity regardless of OGA protein levels (−30 %, $p = 0.04$) (Fig. 2C). Intriguingly, TMG treatment led also to the increased expression levels of OGT in Eu and Ts2 mice after TMG treatment (Fig. 2A and D), probably as compensatory homeostatic mechanism. In consideration that the brain from people with DS demonstrate a pronounced alterations of metabolic profile shifting towards a more energy-inefficient fermentative metabolism [44], we focused our attention on the activation state of AMPK protein and on its role in regulating the HBP. AMPK protein levels showed a significant increase in the frontal cortex of Ts2 animals compared to the Eu (+137 %, $p = 0.0003$), along with a notable reduction following TMG treatment (−123 %, $p < 0.001$) (Supplementary Fig. 2A). However, AMPK activity measured by the ratio between T172 phosphorylation and protein levels showed, on the contrary, a significant decrease in Ts2 compared to Eu mice (−57 %, $p = 0.006$) with a recovery observed after TMG treatment (+40 %, $p = 0.04$) (Fig. 2E and F). GFAT1, the rate-limiting enzyme of the HBP, is negatively regulated by AMPK via inhibitory phosphorylation at S243. The analysis of both GFAT1 protein

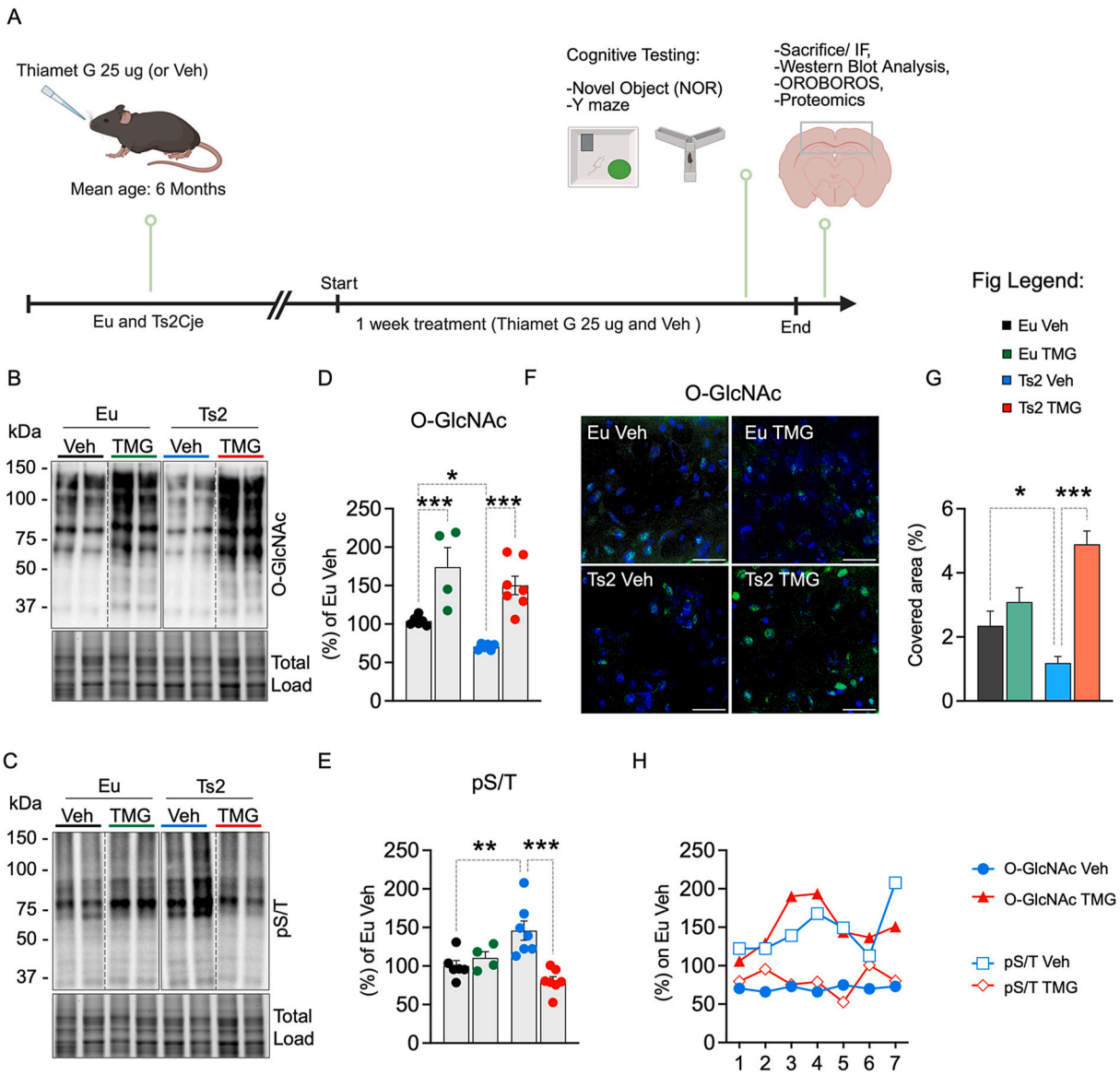

Fig. 1. Intranasal TMG administration reduce OGA activity and increase total O-GlcNAc levels in the frontal cortex of DS mice (A) Schematic representation of the short-term TMG intranasal treatment. 6-month-old animals were treated twice a day with vehicle solution (Veh; PBS 1X solution) or TMG (25 μg Thiamet G solution) for 5 days. Animals were divided according to their genotype and intranasal treatment received in the following groups: Eu Veh, Ts2 Veh, Eu TMG, Ts2 TMG. Mice underwent to behaviour analysis and then samples were collected for the biochemical analysis. **(B and C)** Representative WB images and densitometric evaluation of **(D)** O-GlcNAc in Euploid (Eu) and Ts2 mice treated with Veh or TMG **(E)** pS/T total expression levels. **(F)** Representative confocal immunofluorescence images of O-GlcNAc (green) (scale bar: 10 μm, DAPI for nuclei visualization in Blue) in Eu and Ts2 mice treated with Veh or TMG.**(G)** Quantification of O-GlcNAc signals at single cell level in Eu and Ts2 upon the treatments described above. **(H)** Single data evaluation of O-GlcNAc and pS/T values in Ts2 mice. The graph illustrates the inverse relationship between O-GlcNAc levels and pS/T values measured in the same samples. Data are presented as means ± SEM. Statistical significance was determined using One-way ANOVA with Fisher's LSD test.

levels and phosphorylation at S243 revealed a significant increase in Ts2 TMG mice (+70 % vs. Ts2 Veh, p = 0.01; +43 % vs. Ts2 Veh, p = 0.04) (Fig. 2G and Supplementary Fig. 2B). Nevertheless, GFAT1 inhibition measured by S243 phosphorylation levels, normalized on protein expression levels, showed no significant differences (Fig. 2H).

3.2. *Proteomic analysis identify protein-specific improvements of O-GlcNAc levels in Ts2 mice after TMG treatment*

To detect proteins with a significant increase of O-GlcNAc levels after TMG treatment we performed a MS based proteomics analysis using 2-DE SDS PAGE methodology, as previously published [17]. By image analysis we recognized spots with increased O-GlcNAcylation (Fig. 3A) that have been subsequently identified by MS analysis in 120 different proteins and/or isoforms, as reported in Supplementary Table 3 and detailed in Supplementary Table 4. The MS dataset have been analyzed by different software and/or database to determine their identity, localization, function, roles and interactions. Using the PANTHER Version 19.0 classification system, we aimed to identify key attributes from our dataset including sub-cellular localization, biological processes, molecular function (using GO terms annotated on the trees by the GO Phylogenetic Annotation Project) and protein classes (Fig. 3B.1-B.4) (Supplementary tables 5-8). The subcellular localization analysis revealed that approximately 47 % are cytoplasmatic proteins, while about 16 % are mitochondrial protein and about 7 % are nuclear proteins (Fig. 3B.1). The amount of mitochondrial protein modulated by TMG is increased in respect of what expected following literature studies [45]. The biological process analysis demonstrates that most of the

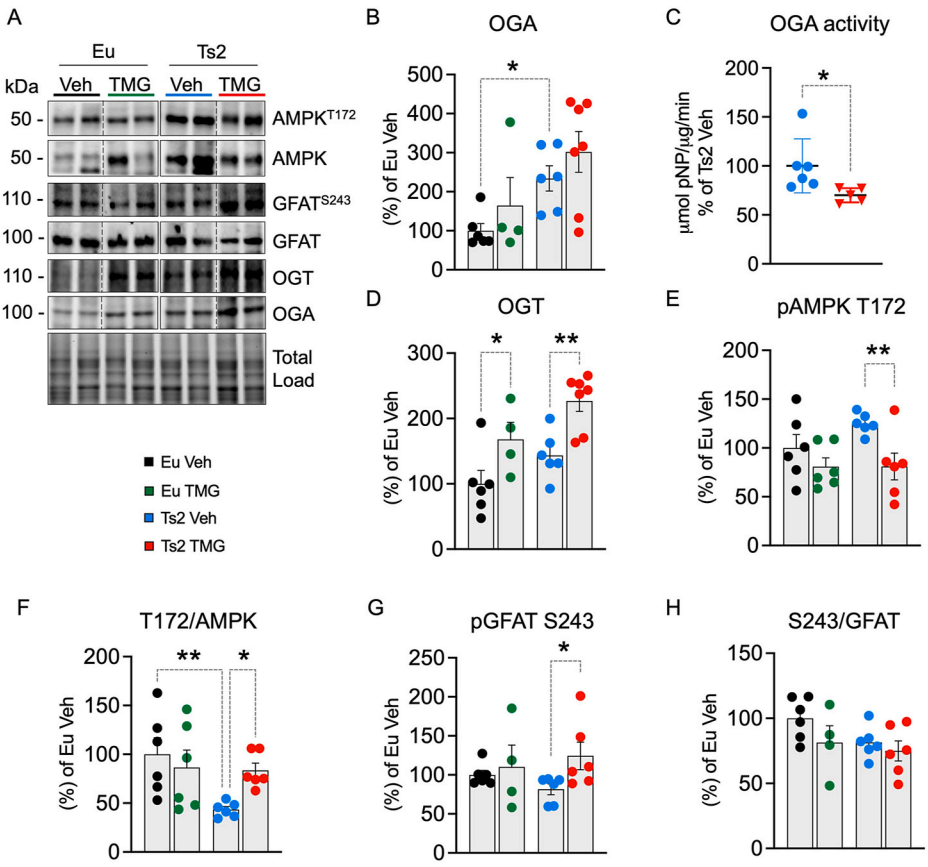

Fig. 2. Intranasal TMG administration reduce OGA activity and regulates AMPK/GFAT1 axis. (A) Representative WB images and densitometric evaluation of **(B)** OGA protein levels, **(C)** OGA activity assay (specific OGA activity is obtained through the normalization on the respective protein levels) **(D)** OGT protein levels. **(E)** Densitometric evaluation of pT172AMPK **(F)** AMPK activation (evaluated as pT172/AMPK ratio). **(G)** pS243 GFAT and **(H)** GFAT activation (evaluated as pS243/GFAT ratio). Data are presented as means ± SEM. Statistical significance was determined using One-way ANOVA with Fisher's LSD test.

proteins are involved in cellular processes (GO:0009987) (36 %) and metabolic processes (16 %) (GO:0008152) (Fig. 3B.2). The molecular analysis shows that 31 % are binding proteins (GO:0005488) while the 26 % have catalytic activity (GO:0003824) (Fig. 3B.3). At final, the protein class analysis demonstrates that proteins identified by MS analysis belongs to the classes of metabolite conversion enzyme (PC00262) (23 %); cytoskeletal proteins (PC00085) (17 %); membrane traffic proteins (PC00150) (8 %); and protein modifying enzyme, (PC00260) (6 %).

Using the STRING version 12.0 knowledgebase and software tool we built the interaction network map and the KEGG databases pathways (Fig. 3C and D) (Supplementary Tables 9-11). The interaction network map report 122 nodes among the identified proteins showing more interactions than what would be expected and suggesting that identified proteins are at least partially biologically connected, as a group (Fig. 3C). Additionally, a detailed in-depth analysis of metabolism alterations by KEGG metabolic pathway analysis (Fig. 3D) support that increased O-GlcNAc levels could significantly affect both catabolic and anabolic processes, particularly in carbohydrate metabolism (Glycolysis and Gluconeogenesis) and amino acid metabolism (arginine/proline metabolism). By REACTOME knowledgebase we built the REACTOME pathway list that suggests that elevated protein O-GlcNAc levels may impact processes involved in mitochondrial protein degradation, PKR-mediated signaling, RHO GTPases activate IQGAPs and aggrephagy, among others (Fig. 3E). The REACTFOAM representation further support the involvement of cellular stress responses and mitochondrial functionality (Fig. 3F) in the rescue of O-GlcNAc levels by TMG.

Finally, to have a more compelling indication on the impact of TMG administration on DS cortical pathways and disease progression we analyzed our database using the Ingenuity Pathway analysis (IPA; Qiagen). IPA allow to identify canonical pathways and downstream effects associated to diseases and functions, as well as selected protein interaction networks (Fig. 4) (Supplementary tables 12-14). The significance values (p-value of overlap) for the canonical pathways are calculated by the right-tailed Fisher's Exact Test. The results show that the increase in the O-GlcNAcylated proteins after TMG treatment is associated with canonical pathways that includes: 14-3-3 mediated signalling, phagosome maturation, glycolysis, mitochondrial dysfunction, ketolysis, synaptogenesis signalling pathways, protein ubiquitination pathway, p70S6K signalling and chaperone mediated autophagy signalling pathway (Fig. 4A). Intriguingly, focusing on mitochondrial pathways, our data reveal the modulation of mitochondrial protein degradation, mitochondrial protein import, ER-mitochondrial signaling pathways, mitochondrial biogenesis, oxidative phosphorylation (OXPHOS) and electron transport chain (ETC), and TCA cycle. In addition, the **Stacked Bar** also highlights changes for other smaller canonical pathways (in components number), mainly metabolic, such as glutamate degradation or aspartate biosynthesis, following O-GlcNAc rescue. Nonetheless, the modulation of endoplasmic reticulum (ER) stress pathways, the Unfolded Protein Response and NRF2 antioxidant response is also observed in TMG-treated DS mice. The IPA analysis further validate and confirm the analysis of our dataset obtained using the REACTOME and the KEGG metabolic database software. Subsequently, we performed through IPA the downstream effects analysis that enables to quickly visualize biological trends and predictions on the role of increased O-GlcNAc levels in preserving/promoting biological processes alterations and diseases. This analysis based on causal effects between molecules and functions suggest that the increase of protein O-GlcNAcylation may

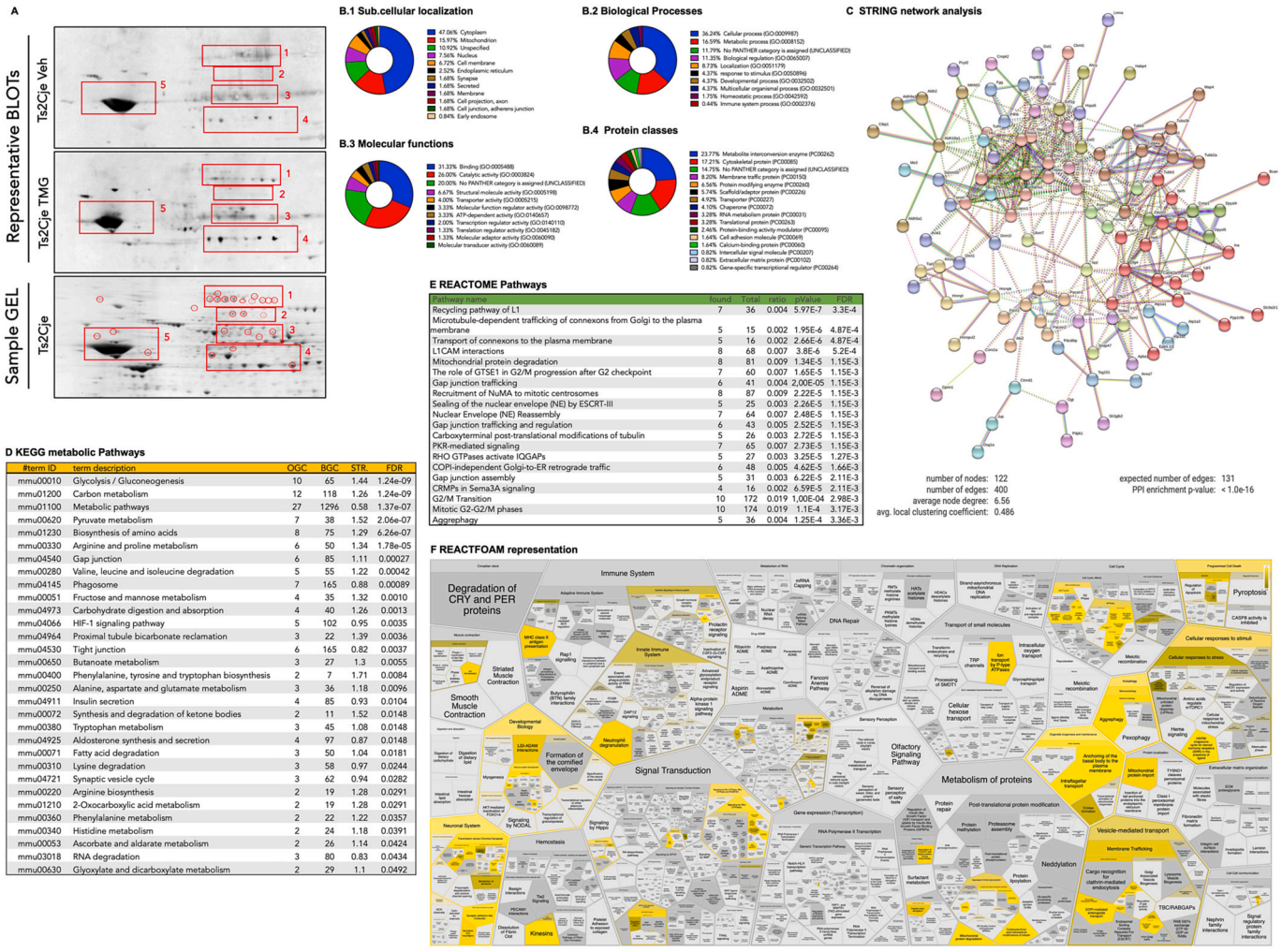

D KEGG metabolic Pathways

#term ID	term description	OGC	BGC	STR	FDR
mmu00010	Glycolysis / Gluconeogenesis	10	65	1.44	1.24e-09
mmu01200	Carbon metabolism	12	118	1.26	1.24e-09
mmu01100	Metabolic pathways	27	1296	0.58	1.37e-07
mmu00620	Pyruvate metabolism	7	38	1.52	2.06e-07
mmu01230	Biosynthesis of amino acids	8	75	1.29	6.26e-07
mmu00330	Arginine and proline metabolism	6	50	1.34	1.78e-05
mmu04540	Gap junction	6	85	1.11	0.00027
mmu00280	Valine, leucine and isoleucine degradation	5	55	1.22	0.00042
mmu04145	Phagosome	7	165	0.88	0.00089
mmu00051	Fructose and mannose metabolism	4	35	1.32	0.0010
mmu04973	Carbohydrate digestion and absorption	4	40	1.26	0.0013
mmu04066	HIF-1 signaling pathway	5	102	0.95	0.0035
mmu04964	Proximal tubule bicarbonate reclamation	3	22	1.39	0.0036
mmu04530	Tight junction	6	165	0.82	0.0037
mmu00650	Butanoate metabolism	3	27	1.3	0.0055
mmu00400	Phenylalanine, tyrosine and tryptophan biosynthesis	2	7	1.71	0.0084
mmu00250	Alanine, aspartate and glutamate metabolism	3	36	1.18	0.0096
mmu04911	Insulin secretion	4	85	0.93	0.0104
mmu00072	Synthesis and degradation of ketone bodies	2	11	1.52	0.0148
mmu00380	Tryptophan metabolism	3	45	1.08	0.0148
mmu04925	Aldosterone synthesis and secretion	4	97	0.87	0.0148
mmu00071	Fatty acid degradation	3	50	1.04	0.0181
mmu00310	Lysine degradation	3	58	0.97	0.0244
mmu04721	Synaptic vesicle cycle	3	62	0.94	0.0282
mmu00220	Arginine biosynthesis	2	19	1.28	0.0291
mmu01210	2-Oxocarboxylic acid metabolism	2	19	1.28	0.0291
mmu00360	Phenylalanine metabolism	2	22	1.22	0.0357
mmu00340	Histidine metabolism	2	24	1.18	0.0391
mmu00053	Ascorbate and aldarate metabolism	2	26	1.14	0.0424
mmu03018	RNA degradation	3	80	0.83	0.0434
mmu00630	Glyoxylate and dicarboxylate metabolism	2	29	1.1	0.0492

E REACTOME Pathways

Pathway name	found	Total	ratio	pValue	FDR
Recycling pathway of L1	7	36	0.004	5.97E-7	3.3E-4
Microtubule-dependent trafficking of connexons from Golgi to the plasma membrane	5	15	0.002	1.95E-6	4.87E-4
Transport of connexons to the plasma membrane	5	16	0.002	2.66E-6	4.87E-4
L1CAM interactions	8	68	0.007	3.8E-6	5.2E-4
Mitochondrial protein degradation	8	81	0.009	1.34E-5	1.15E-3
The role of GTSE1 in G2/M progression after G2 checkpoint	7	60	0.007	1.65E-5	1.15E-3
Gap junction trafficking	6	41	0.004	2,00E-05	1.15E-3
Recruitment of NuMA to mitotic centrosomes	8	87	0.009	2.22E-5	1.15E-3
Sealing of the nuclear envelope (NE) by ESCRT-III	5	25	0.003	2.26E-5	1.15E-3
Nuclear Envelope (NE) Reassembly	7	64	0.007	2.48E-5	1.15E-3
Gap junction trafficking and regulation	6	43	0.005	2.52E-5	1.15E-3
Carboxyterminal post-translational modifications of tubulin	5	26	0.003	2.72E-5	1.15E-3
PKR-mediated signaling	7	65	0.007	2.73E-5	1.15E-3
RHO GTPases activate IQGAPs	5	27	0.003	3.25E-5	1.27E-3
COPI-independent Golgi-to-ER retrograde traffic	6	48	0.005	4.62E-5	1.66E-3
Gap junction assembly	5	31	0.003	6.22E-5	2.11E-3
CRMPs in Sema3A signaling	4	16	0.002	6.59E-5	2.11E-3
G2/M Transition	10	172	0.019	1,00E-04	2.98E-3
Mitotic G2-G2/M phases	10	174	0.019	1.1E-4	3.17E-3
Aggrephagy	5	36	0.004	1.25E-4	3.36E-3

Fig. 3. 2-DE proteomics analysis of protein showing O-GlcNAcylation changes after TMG administration in Ts2 mice. (A) Representative 2-DE blot images with a focus on the areas with abundant changes in protein O- GlcNAc levels between Veh-treated (top image) and TMG-treated (middle image) Ts2 mice. On the bottom a representative Gel image shows specific spots identified by MS. **(B.1–4)** Pie graphs reporting subcellular localizations **(B.1)**, biological processes **(B.2)**, molecular functions **(B.3)** and protein classes **(B.4)** of proteins identified by MS and analyzed by PANTHER classification system. **(C)** Interactions and network analysis of identified proteins by STRING analysis. **(D)** KEGG metabolic pathways lists identified by STRING analysis. The table reports the pathway identification number (# term ID), the pathway description (term description) the observed gene count (OGC), the biological gene count in the pathway (BGC), the strength (STR) and the false discovery rate (FDR). **(E)** REACTOME pathway table reporting pathway name, protein found, total and found/total ratio, p-value, FDR, species name. **(F)** REACTFOAM representation highlighting principal functions and pathways associated with increased O-GlcNAc levels ($p < 0.05$).

have prominent role in ameliorating the neurodegenerative process occurring in DS mice. It shows a strong impact on downstream effects such as neurological diseases, nervous system development and function, cell death and survival, molecular transport and post-translational modification (Fig. 4B). Notably the most significant functions within neurological diseases category includes abnormal morphology of nervous system (Fig. 4B.1) but also amyloid beta accumulation and tauopathy in neurons. These findings highlight the potential of restoring protein O-GlcNAc levels as a strategy to mitigate brain degeneration and reduce the progression of Alzheimer's disease-related pathology. Furthermore, the evaluation of selected networks (Fig. 4C) built from the analysis of molecules interactions by IPA demonstrate that increased O-GlcNAc levels occurs on proteins potentially involved in the regulation of behaviour and of cellular development, growth and proliferation, as well as, of cell-to-Cell signalling and interaction, and nervous system development and function.

3.3. *TMG treatment rescues mitochondrial bioenergetics*

The disruption of mitochondrial homeostasis, due to widespread downregulation and altered PTMs of proteins involved in OXPHOS, is a major contributor to DS neurodegeneration [25,26,46,47]. O-GlcNAcylation dynamically modifies numerous mitochondrial proteins, influencing energy metabolism [48]. Modulating O-GlcNAc levels has been shown to impact both mitochondrial bioenergetic function and structural integrity [49–51]. Based also on proteomics data that support the modulation of mitochondrial pathways associated with homeostasis and metabolism, we evaluated, in murine brain samples, mitochondrial activity through the analysis of the oxygen consumption rate (OCR) using the OROBOROS (Fig. 5A–D). We found a significant increase for Complex I activity in Ts2 TMG mice (+3.2 pmol/s/mg protein vs. Ts2 Veh, $p = 0.03$) (Fig. 5E). No significant changes were observed for Complex II (Fig. 5F). While a trend of increase was observed for Complex IV (+30 pmol/s/mg protein vs. Ts2 Veh, $p = 0.06$) (Fig. 5G). To determine whether mitochondrial activity was influenced by alterations in the expression of ETC complexes, we assessed the protein levels of their subunits. Our findings revealed a consistent reduction in NDUFB8 subunit (Complex I) levels observed in the Ts2 Veh mice (−44 % vs. Eu Veh, $p = 0.04$) (Fig. 5I). Remarkably, TMG treatment significantly increased NDUFB8 levels in Ts2 mice (+74 % vs. Ts2 Veh, $p = 0.001$), as well as

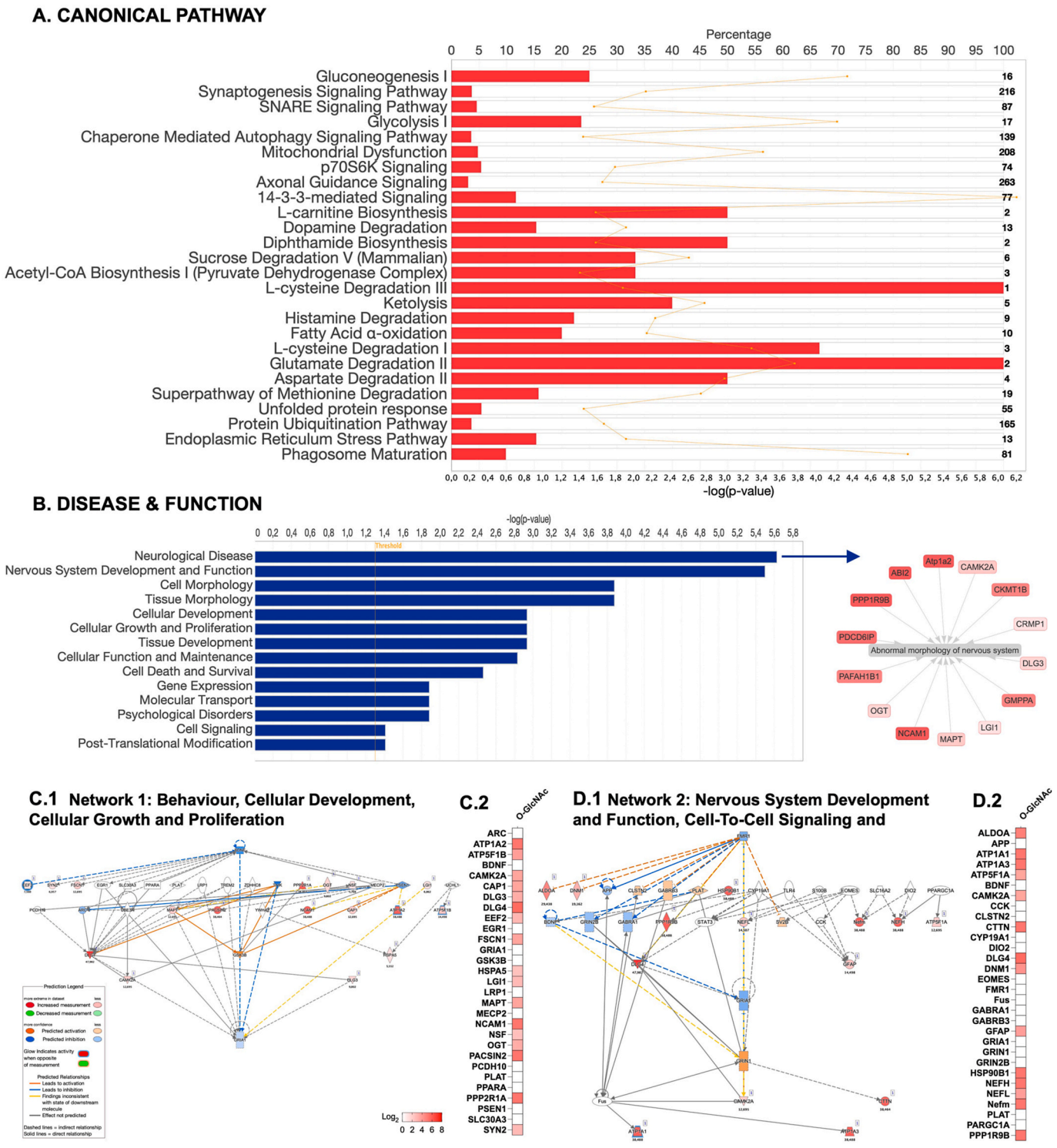

Fig. 4. Ingenuity Pathway analysis of 2-DE-identified proteins with changes in O-GlcNAc levels after TMG treatment in Ts2 mice. (A) Canonical Pathway analysis by IPA software listed according to significance (-log(p-value)), total gene count and gene count percentage in the pathway. **(B)** Downstream effects analysis by IPA analysis highlighting diseases and functions significantly influenced by changes in O-GlcNAc levels of proteins identified by MS and listed according to significance (-log(p-value)). **B.1** Radial diagram showing protein whose increase in O-GlcNAc levels promote changes of abnormal morphology of nervous system network within neurological disease category. **(C)** Specific network identified by IPA software with interaction nodes **(C.1 and D.1)** and the levels of O-GlcNAc modification for the components of the networks **(C.2 and D.2)**.

SDHB subunit (Complex II) levels (+39 % vs. Ts2 Veh, p = 0.01) (Fig. 5I and J). However, no significant differences were observed for UQCRC2 subunit (Complex III) or MTCO1 subunit (Complex IV) and ATP5A subunit (Complex V) (Fig. 5K–M). To determine whether the changes in mitochondrial protein complexes subunits was associated with elevated O-GlcNAcylation within the mitochondrial compartment, we isolated mitochondria and assessed the levels of O-GlcNAc and the expression of OGT/OGA. The mitochondrial analysis reveals a significant increase of O-GlcNAc in Ts2 TMG (+48 % vs. Ts2 Veh, p = 0.01) (Fig. 6B). Mitochondrial subcellular fractionation identified the presence of two

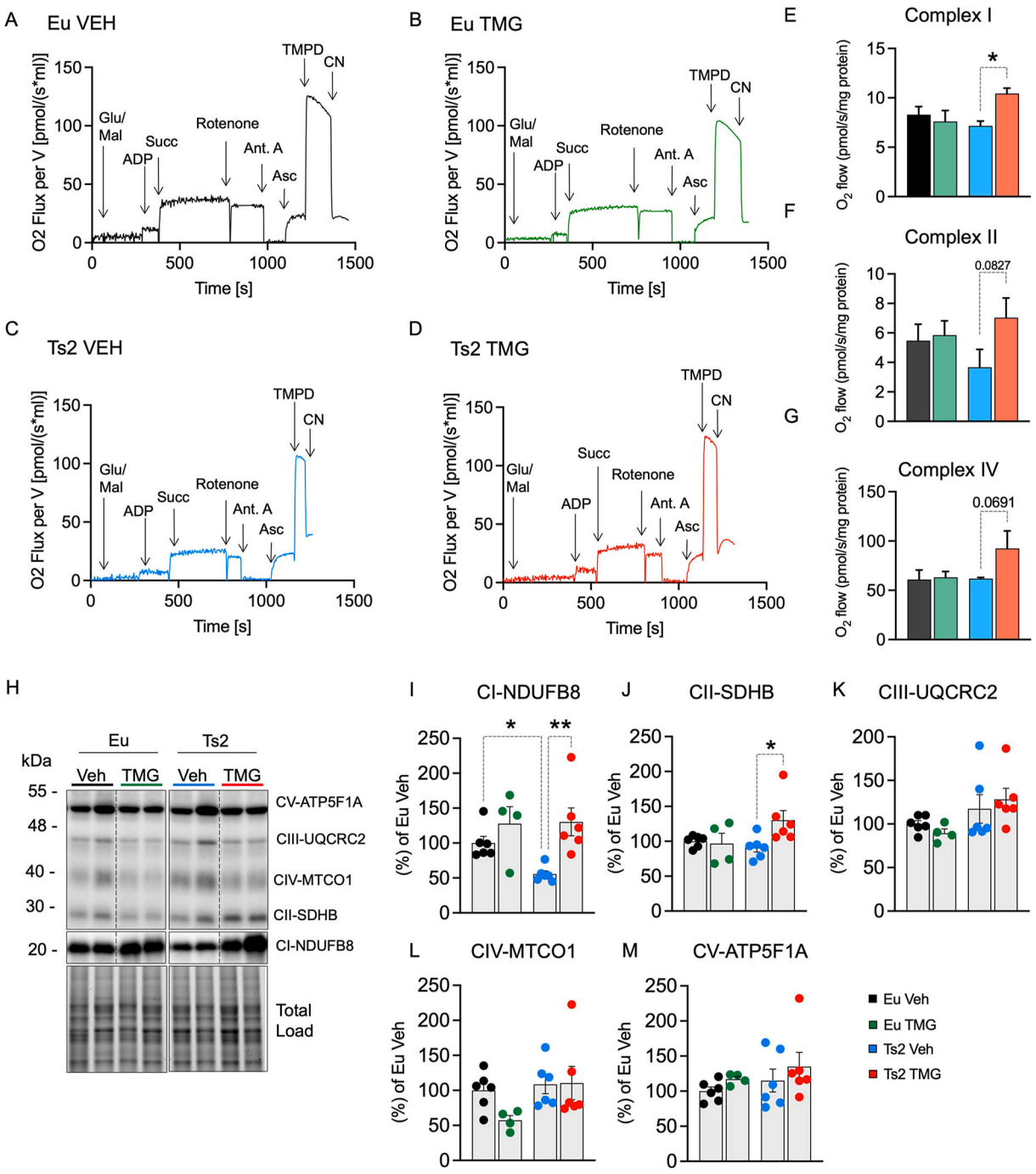

Fig. 5. TMG enhance mitochondrial metabolism in the frontal cortex of Ts2 mice. **(A–D)** Representative traces showing oxygen consumption rates (OCR) of mitochondria isolated from Eu and Ts2 mice treated with Veh or TMG. Arrows indicate the addition of substrates and/or inhibitors to the chamber containing mitochondria and 10 mM Glutamate, 2 mM Malate (5 mM ADP, 5 mM Succinate, 2.5 μM Antimycin, 2 mM Ascorbate, 0.8 mM TMPD and 1 mM Sodium Cyanide (CN). Quantification of the OCR, normalized for protein content (pmol O_2/s/mg proteins) after the addition of ADP in the presence of Glutamate-Malate **(E)** (Complex I); **(F)** Succinate subtracted for Rotenone (Complex II); **(G)** Antimycin to block Complex III, Ascorbate and TMPD, and NaCN to subtract cyanide-insensitive O_2 consumption rate (Complex IV). Data are presented as means ± SEM. Statistical significance was determined using One-way ANOVA with Fisher's LSD test. Mitochondrial OXPHOS complexes subunits protein levels were evaluated in the frontal cortex of Eu and Ts2 mice treated with Veh or TMG **(H)** Representative WB images and densitometric evaluation of **(I)** Complex I (subunit NDUFB8), **(J)** Complex II (subunit SDHB), **(K)** Complex III (subunit UQCRC2), **(L)** Complex IV (subunit MTCO1), **(M)** Complex V (subunit ATP5A). Values are given as percentage of Eu set as 100 %. Data are presented as means ± SEM. Statistical significance was determined using One-way ANOVA with Fisher's LSD test.

different isoforms of OGA: the long (L-OGA) and the short (S-OGA) isoform. Quantification reveals a significant reduction of the S-OGA in Ts2 TMG (+41 % vs. Ts2 Veh, p = 0.04) (Fig. 6C). Consistent with the findings of Pagesy et al. [52], we demonstrate that the S-OGA is preferentially localized in the mitochondria-enriched fraction and is modulated by TMG. Conversely, OGT protein levels were significantly increased in the mitochondria fraction of Ts2 following TMG treatment (+25 % vs. Ts2 Veh, p = 0.04) (Fig. 6D). No changes in nuclear O-GlcNAc levels or in OGT and OGA expression were observed (Fig. 6E–G). Furthermore, to evaluate whether reduced S-OGA levels

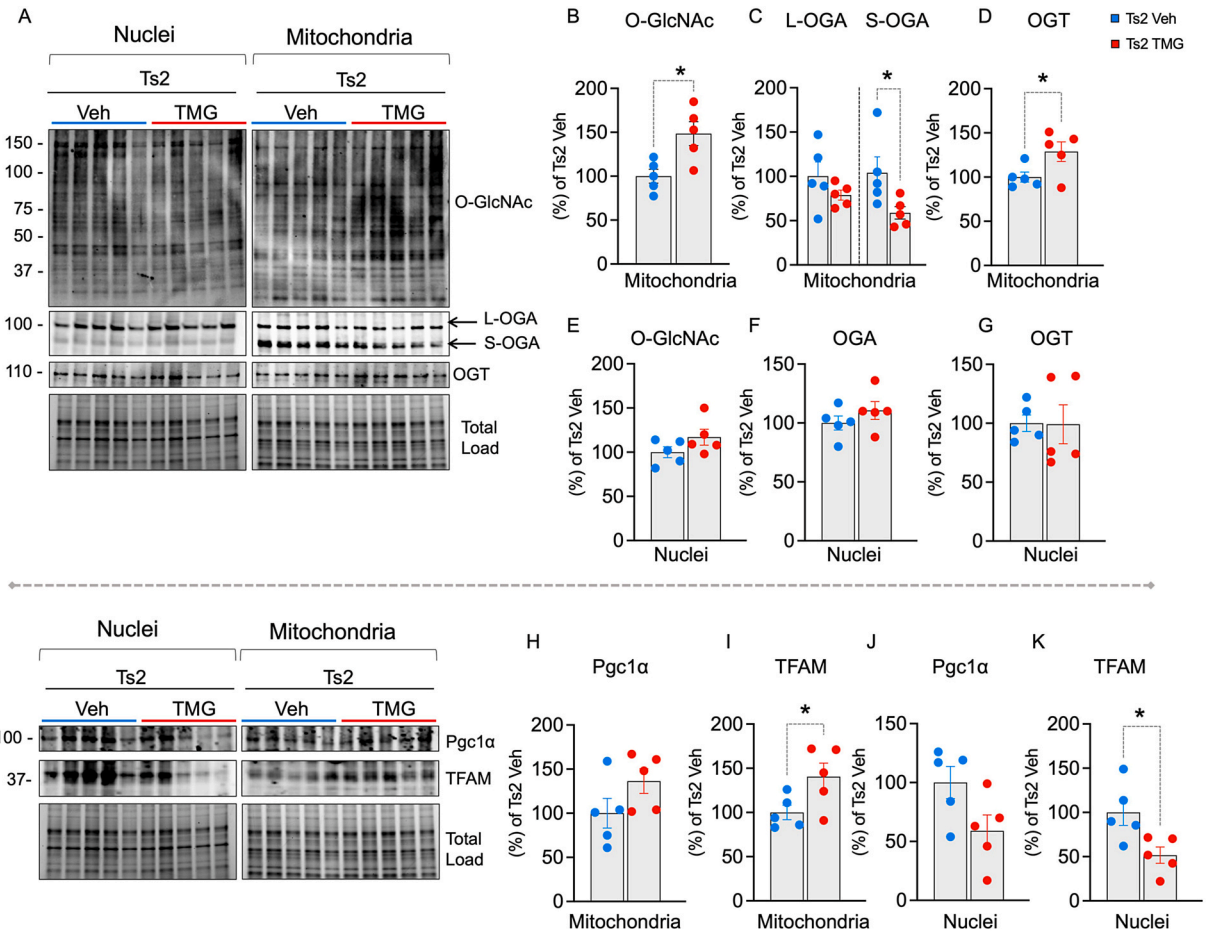

Fig. 6. Evaluation of O-GlcNAc cycle in mitochondrial and nuclear factions after TMG treatment. Evaluation of O-GlcNAc, OGA, OGT, PGC1a and TFAM following subcellular fractionation of cortical tissue collected from Ts2 mice treated with Veh and TMG (n = 5 independent samples/group). **(A)** Representative WB images and densitometric evaluation of **(B and E)** O-GlcNAc, **(C and F)** OGA, L-OGA and S-OGA, **(D and G)** OGT **(H and J)** Pgc1a and **(I and K)** TFAM in the mitochondrial and nuclear fraction of Ts2 mice treated with Veh and TMG. Purity of the subcellular fractions was determined by examining Complex 1 (Anti-NDUFB8) in the mitochondrial fraction and Histone H3 antibody in the nuclear fraction by WB analysis. The densitometric value are given as percentage of Ts2 Veh set as 100 %. Data are presented as means ± SEM. Statistical significance was determined using Student t-test analysis (*p < 0.05, **p < 0.01).

and increased mitochondrial O-GlcNAc levels affect mitochondrial biogenesis, we assessed two key markers: PGC1α and TFAM. The analysis revealed a slight increase in PGC1α levels and a significant increase in TFAM protein levels in the mitochondrial fraction (+41 % vs. Ts2 Veh, p = 0.04) (Fig. 6H and I). In contrast, no changes in PGC1α were observed in the nuclear fraction, while TFAM levels significantly decreased (+48 % vs. Ts2 Veh, p = 0.02) (Fig. 6J and K).

3.4. TMG treatment improves redox responses and reduces oxidative damage

Previous studies reported an emerging mutual relationship between O-GlcNAc and redox homeostasis [53]. The O-GlcNAc cycle may directly induce antioxidant and stress response cascades, while indirectly it may control ROS production by regulating mitochondrial biogenesis/degradation ratio and mitochondrial function [48,54,55]. Accordingly, canonical pathway analysis supports the modulation of NRF2 response through the increase of the O-GlcNAc levels of HSP90B1, known to associates with antioxidant cascades and NRF2 induction [56]. To further deepen this process, we analyzed BACH1/NRF2 expression levels and nuclear translocation and the expression of downstream targets. The gene coding for BACH1 is triplicated in DS and promote a repression of NRF2 antioxidant pathways, as demonstrated in humans and mice [57]. Intriguingly, previous studies supported that O-GlcNAc modification directly regulate NRF2 activation on S103 and S334, and indirectly through the O-GlcNAcylation of Keap1 or upstream signals [53,58]. Our data show that TMG restores *NRF2* gene expression levels in Ts2 mice (+0.24-fold, p = 0.008), which are reduced in the comparison to Eu controls (−0.17-fold, p = 0.04) (Fig. 7A). Conversely, *BACH1* expression levels are elevated in Ts2 mice (+0.45-fold, p = 0.04), as expected, suggesting the repression of the NRF2-mediated antioxidant response (Fig. 7B). To assess whether the increase in *NRF2* gene expression correlates with enhanced nuclear translocation, we measured NRF2 protein levels in nuclear extracts from Ts2 mice treated with Veh or TMG. TMG treatment led to a clear increase in nuclear NRF2 (+55 %, p = 0.003) (Fig. 7C and D). Though BACH1 protein level remained unchanged (Fig. 7C and E) the increase in nuclear NRF2/BACH1 ratio (+62 %, p = 0.03) supports a shift toward NRF2-driven transcriptional activation (Fig. 7F). Subsequently, we investigated the expression of two NRF2-regulated genes involved in glutathione biosynthesis: *GSS* (glutathione synthetase) and *GCLM* (glutamate-cysteine ligase modifier subunit). *GSS* expression showed a significant increase in Ts2 mice compared to Eu controls (+1.5-fold, p = 0.03) (Fig. 7G). In contrast, although not statistically significant, *GCLM* expression tended to decrease in Ts2 mice in respect to Eu (−0.25-fold, p = 0.06), and this trend was modulated following TMG treatment (+0.25-fold, p = 0.06) (Fig. 7H). In addition, we assessed the expression of HO-1 and NQO1, two canonical NRF2 downstream targets (Fig. 7I and J). HO-1 protein levels were significantly increased in TMG-treated Ts2 mice compared to Veh-treated Ts2 controls (+35 %, p = 0.004) (Fig. 7J),

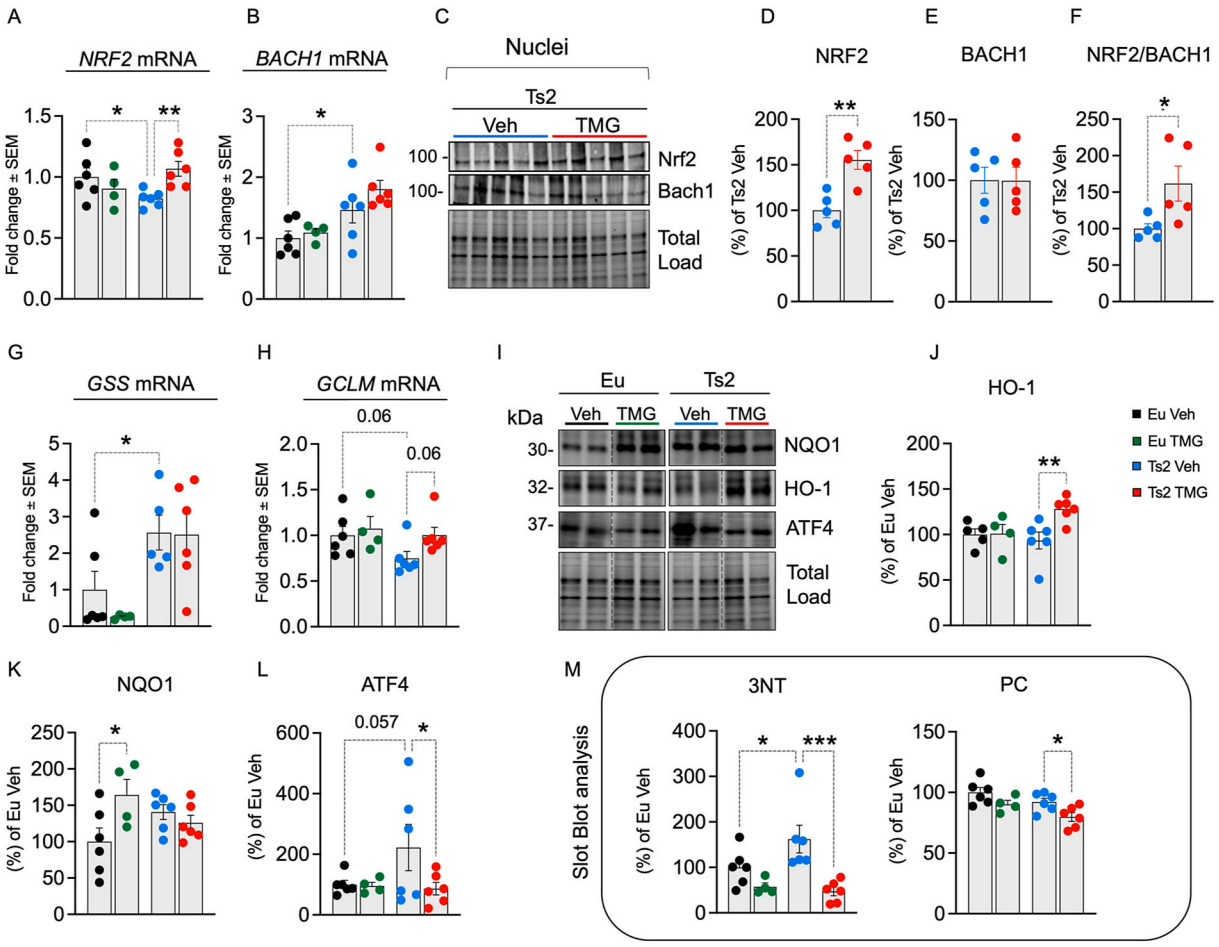

Fig. 7. TMG induce NRF2- related antioxidant pathway, reduce ER-resident stress responses and protect from oxidative damage. **(A and B)** Gene expression data of *NRF2* and *BACH1* in Eu and Ts2 mice treated with Veh or TMG. The gene expression data were normalized to B2M. The fold change was determined via the 2(-ΔΔCt) method. **(C-F)** Evaluation of NRF2 and BACH1 in nuclear fraction following subcellular fractionation of cortical tissue collected from Ts2 mice treated with Veh and TMG (n = 5 independent samples/group). **(G and H)** Gene expression data of *GSS* and *GCLM* in Eu and Ts2 mice treated with Veh or TMG. **(I)** Representative WB images and densitometric evaluation of **(J)** HO-1, **(K)** NQO1 and **(L)** ATF4 **(M)** Densitometric evaluation of oxidative markers, (i.e., 3-NT and PC). in Eu and Ts2 mice treated with Veh or TMG. Data are presented as means ± SEM. Statistical significance was determined using One-way ANOVA with Fisher's LSD test.

supporting the induction of the antioxidant pathway. No significant changes were observed in NQO1 levels in Ts2 mice, while a significant increase was detected in Eu mice following TMG treatment (+64 %, p = 0.003) (Fig. 7K). Furthermore, considering the modulation of the ER stress pathway (Fig. 4A) and of PKR-mediated signaling (Fig. 3E) as described by proteomic analysis, we analyzed the levels of ATF4, an ER-resident protein regulated by O-GlcNAc changes [49]. We observed a trend of induction in Ts2 animals that is significantly reduced upon TMG administration (−136 %, p = 0.03). Finally, to evaluate the impact of TMG on antioxidant and stress responses, we measured two markers of protein oxidative damage: 3-nitrotyrosine (3-NT) and protein carbonyls (PC). Only 3-NT levels were significantly increased in Ts2 mice compared to Eu controls (+62 %, p = 0.03), whereas PC levels remained unchanged. TMG treatment led to a marked reduction in both 3-NT and protein carbonyl levels in Ts2 mice (−15 %, p = 0.0005 and −12 %, p = 0.002, respectively) (Fig. 7M), supporting a functional decrease in oxidative damage following activation of the antioxidant and stress pathway. These results support the association between O-GlcNAc and redox homeostasis through the regulation of NRF2 signaling and ER-resident stress responses.

3.5. TMG administration reduces the phosphorylation of APP and tau

Neuropathological features of AD, such as APP, APP cleavage products, and phosphorylated Tau, begin to build up early in the brains of individuals with DS and corresponding mouse models, serving as neurotoxic initiators [20,23,25,59,60]. Ts2 mice develop genetic- and age-dependent neuropathologic markers displaying increased phosphorylation of APP, at T668, and of Tau, at multiple residues, along with metabolic defects and reduced cognitive performances [18,61,62]. Evidence suggests that elevated pAPP at T668 promotes increased Aβ production by enhancing γ-secretase cleavage [63]. Our results from confocal microscopy analysis support the increase of pAPP T668 in Ts2 Veh vs. Eu Veh (+0.73, p = 0.008), which were significantly reduced following TMG treatment (−0.76, p = 0.01) (Fig. 8A and B). We also observed decreased pAPP T668 levels in Eu TMG mice vs. Eu Veh (−0.78, p = 0.001). Additionally, confocal microscopy analysis showed an increase in colocalization (Manders coefficient) between pAPP T668 and O-GlcNAc signal in Ts2 mice (+0.13, p = 0.01), which was reversed after TMG administration (−0.12, p = 0.01) (Fig. 8C). WB analysis further confirmed the elevation of pAPP T668 in Ts2 Veh (+62 % vs. Eu Veh, p = 0.034), as well as, pAPP T668 reduction in Ts2 after TMG treatment (−57 % vs. Ts2 Veh, p = 0.04) (Fig. 8D and E). A similar trend was observed for APP protein levels (+75 % in Ts2 Veh vs. Eu Veh and −70 % in Ts2 mice after TMG treatment; Fig. 8F). To assess the impact of TMG-related modulation of pAPP T668 on Aβ formation, we analyzed soluble Aβ 1–42 levels. Our analysis reveals a significant decrease in Aβ 1–42 levels in Ts2 TMG mice group in respect of Veh treated mice (−69

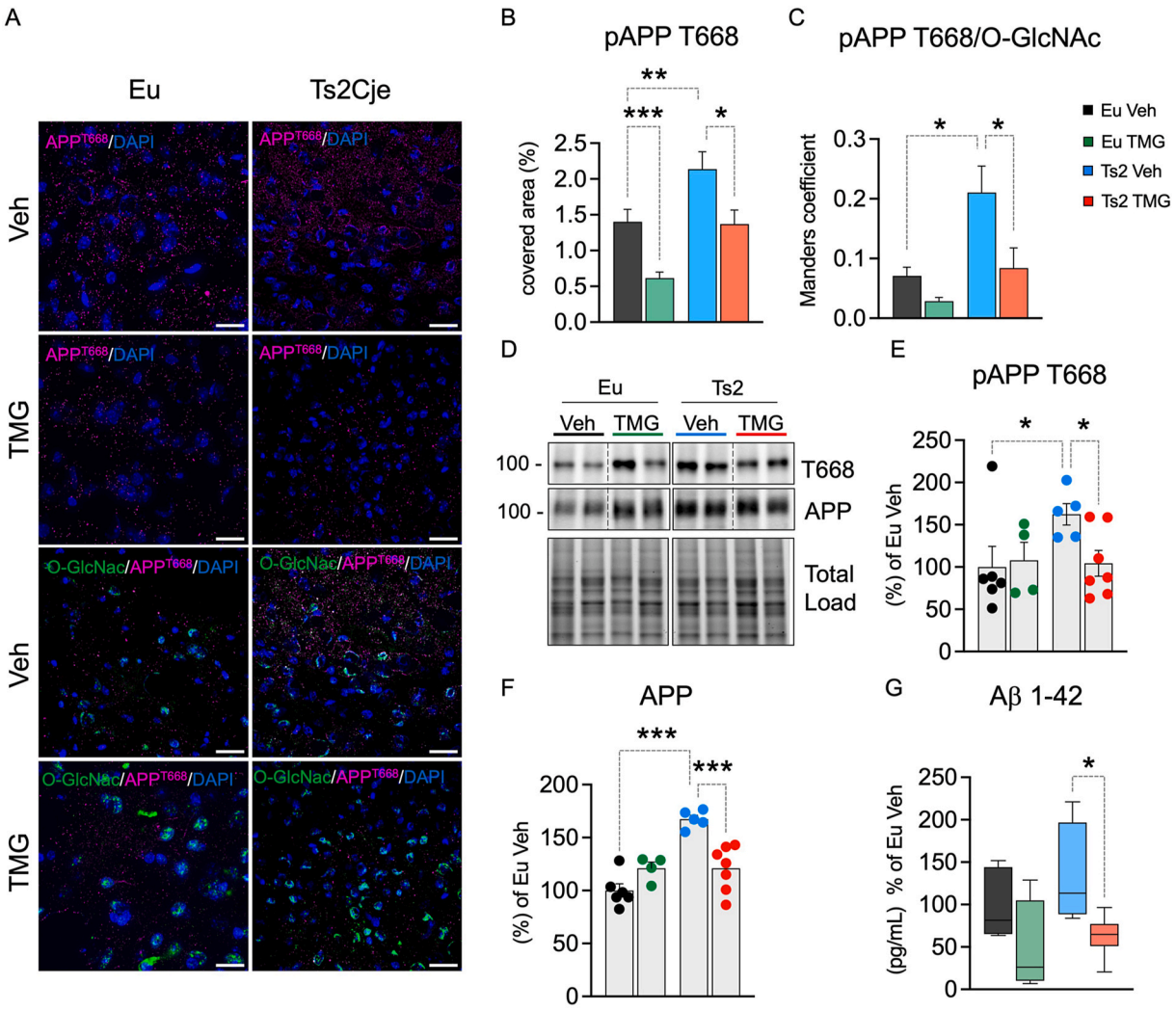

Fig. 8. TMG reduces APP phosphorylation. (A) Representative confocal immunofluorescence images of O-GlcNAc (Green), APP pT668 (Violet) (scale bar: 10 μm, DAPI for nuclei visualization in Blue) in Eu and Ts2 mice treated with Veh or TMG. **(B)** Quantification of APP pT668 signals at single cell level in Eu and Ts2 upon the treatments described above. **(C)** Colocalization analysis of O-GlcNAc (green), APP pT668 (red). Specifically, channels 1 and 2 corresponding to the selected signals were chosen for analysis, and masks were applied to APP pT668 signals to quantify the extent of colocalization with O-GlcNAcylation signals. **(D)** Representative WB images and densitometric evaluation of **(E)** APP pT668 and **(F)** Total APP in Euploid (Eu) and Ts2 mice treated with Veh or TMG. **(G)** Evaluation of soluble Aβ 1–42 peptide by ELISA. Data are presented as means ± SEM. Statistical significance was determined using One-way ANOVA with Fisher's LSD test.

pg/mL) suggesting the potential efficacy of the compound in reducing Aβ load (Fig. 8G).

To further assess the impact of TMG on AD-related pathology, we evaluated Tau phosphorylation through confocal microscopy and WB analysis (Fig. 9). We measured the phosphorylation levels at S202/Y205 (AT8) and T181 residues, which are known to be crucial in the formation of neurofibrillary tangles. Confocal microscopy of pTau AT8 showed a significant decrease in Ts2 mice following TMG treatment (−2.5, $p = 0.005$) (Fig. 9A). Additionally, confocal microscopy analysis showed an increase in colocalization of pTau AT8 and O-GlcNAc signals in Ts2 veh mice vs. Eu veh (+0.09, $p = 0.004$), which was reduced in Ts2 TMG vs. Ts2 Veh (−0.1, $p = 0.0005$) (Fig. 9C). Intriguingly, although the degree of colocalization between phosphorylation and O-GlcNAcylation signals are modest, the statistically significant changes observed following TMG treatment suggests a biologically relevant shift. Intriguingly, this level of spatial overlap suggests direct co-occupancy rather than cooperation, thus the colocalization signal likely reflects a subset of molecules transitioning between the post-translational states [12]. WB analysis on pTau T181 demonstrates increased levels in Ts2 Veh mice (+42 % vs. Eu Veh, $p = 0.01$), while a reduction is observed in Ts2 mice after TMG administration (32 %; $p = 0.04$) (Fig. 9D and E). Notably we report an increase of T181 in Eu mice after TMG treatment that may suggests a compensatory homeostatic effect to adapt to elevated O-GlcNAc levels. This result aligns with the lack of correlation observed between T181 and GlcNAc in humans non-disease cases [64]. To note, Tau protein detected in Ts2 mice corresponds to endogenous murine Tau, as these animals do not express human Tau. This distinction is important when comparing findings with AD models that overexpress human Tau isoforms. The analysis of total Tau levels demonstrates a significant increase in Ts2 mice compared to Eu mice, as reported in the literature [61], with no further differences observed after treatment (Fig. 9F). The reduction in colocalization of protein O-GlcNAcylation with APP or Tau phosphorylation following TMG treatment suggests that TMG modulates the mutual relationship between O-GlcNAc and phospho residues, which may significantly affect protein function and stability.

3.6. TMG treatment improves recognition memory

To investigate the impact of increased O-GlcNAc levels on recognition and spatial memory deficits in Ts2 mice, we performed the NOR and Y-maze tests. Ts2 mice are known to develop pronounced memory impairments starting at 6 months of age [23,65]. Data from the NOR test

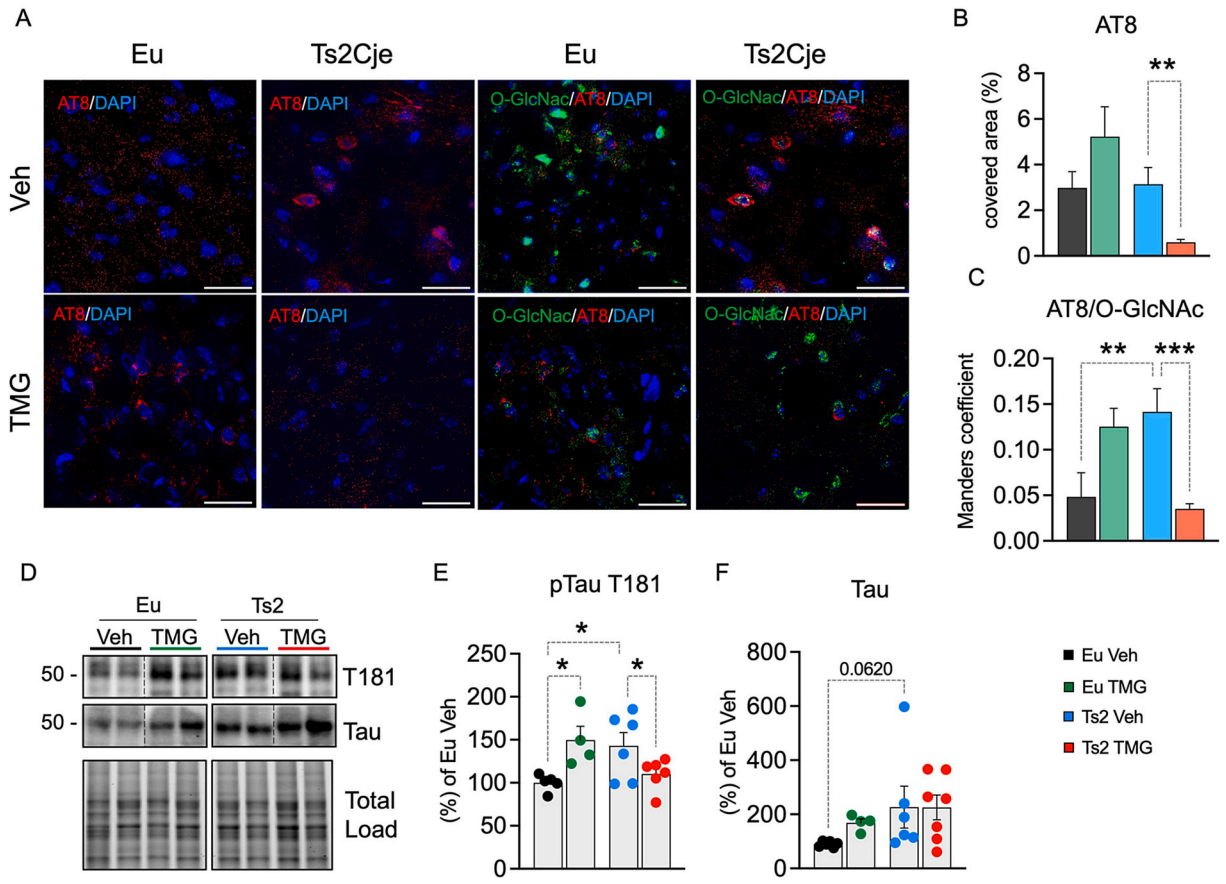

Fig. 9. TMG reduces Tau phosphorylation. (A) Representative confocal immunofluorescence images of O-GlcNAc (green), AT8 (red) (scale bar: 10 μm, DAPI for nuclei visualization in Blue) in Eu and Ts2 mice treated with Veh or TMG. **(B)** Quantification of AT8 signals at single cell level in Eu and Ts2 upon the treatments described above. **(C)** Colocalization analysis of O-GlcNAc (green), AT8 (red). Specifically, channels 1 and 2 corresponding to the selected signals were chosen for analysis, and masks were applied to AT8 signals to quantify the extent of colocalization with O-GlcNAcylation signals. **(D)** Representative WB images and densitometric evaluation of **(E)** TauT181 and **(F)** Total Tau in Eu and Ts2 mice treated with Veh or TMG. Data are presented as means ± SEM. Statistical significance was determined using One-way ANOVA with Fisher's LSD test.

indicate that Eu mice exhibit a preference index (PI) exceeding 50 %, whereas Ts2 mice (Veh groups) display a PI below 50 % (Fig. 10B). Remarkably, TMG treatment successfully increase the PI in Ts2 mice (+15 % vs. Ts2 TMG, p = 0.01; Fig. 10B). The evaluation of the discrimination index (DI) demonstrates a significant reduction in Ts2 mice (−0.32 vs. Eu, p = 0.02) which was rescued following TMG administration (+0.31 vs. Eu, p = 0.01) (Fig. 10C). NOR results suggest a recovery of recognition memory after 5 days of TMG administration. In contrast, the Y-maze test revealed no significant differences in spatial memory as assessed by the DI (Supplementary Fig. 3A). Additionally, the total number of entries in the Y-maze did not differ significantly between groups, suggesting that general locomotor activity remained consistent across conditions (Supplementary Fig. 3B). The differential outcomes on cognitive testing might be related to the length of the administration protocol and/or to the different memory domains evaluated.

4. Discussion

Changes of O-GlcNAcylation are highly context-dependent and can either activate or inhibit protein function by modulating protein stabilization, protein-protein interactions, catalytic activity, and protein degradation, often through crosstalk with other PTMs such as phosphorylation [5]. Elevating O-GlcNAc levels has shown promise as a therapeutic approach for slowing neurodegeneration, as it regulates several pathways linked to cellular toxicity and cognitive decline [13,28,43,66]. Nonetheless, the precise molecular mechanisms responsible for its neuroprotective effects have not been fully elucidated. In the present study we investigated the mechanisms by which TMG-induced restoration of O-GlcNAc levels promotes behavioral and molecular improvements in a murine model of DS. Previous studies from our group showed, for the first time, that the reduction of O-GlcNAc levels was associated with energy defects and pathological hallmarks in the brain of DS and high fat diet-treated mice [18,29]. Here we report that short-term TMG treatment ameliorates recognition memory deficits and rescues mitochondrial impairments and pathological signatures in DS mouse brain. Further, our data support that TMG not only facilitates the recovery of specific proteins exhibiting reduced O-GlcNAcylation, but it may act globally promoting improvements in neuronal function across multiple pathways. Indeed, while evidence strongly supports the primary benefit of reducing neuropathological hallmarks associated with APP and Tau, it is crucial not to underestimate the potential role of TMG in alleviating other defective processes known to promote AD development. These include neuronal signaling, energy production, and stress responses, known to be impaired in AD but also influenced by protein O-GlcNAcylation. O-GlcNAc levels plays a critical role in brain bioenergetics, essential for maintaining neuronal function and resilience [29,43,49,55,67,68]. Studies on DS brain highlighted an early reduction of glucose uptake and the development of insulin resistance, which are linked to reduced HBP flux and aberrant protein O-GlcNAcylation levels [18]. In turn, the chronic disturbance in O-GlcNAc cycling caused by nutrient imbalances may worsen synaptic dysfunction, metabolic alterations and mitochondrial failure, ultimately promoting neurodegenerative features [68]. In this work, we confirm the concomitant alteration of OGA expression and AMPK/GFAT1 regulation as genetic and

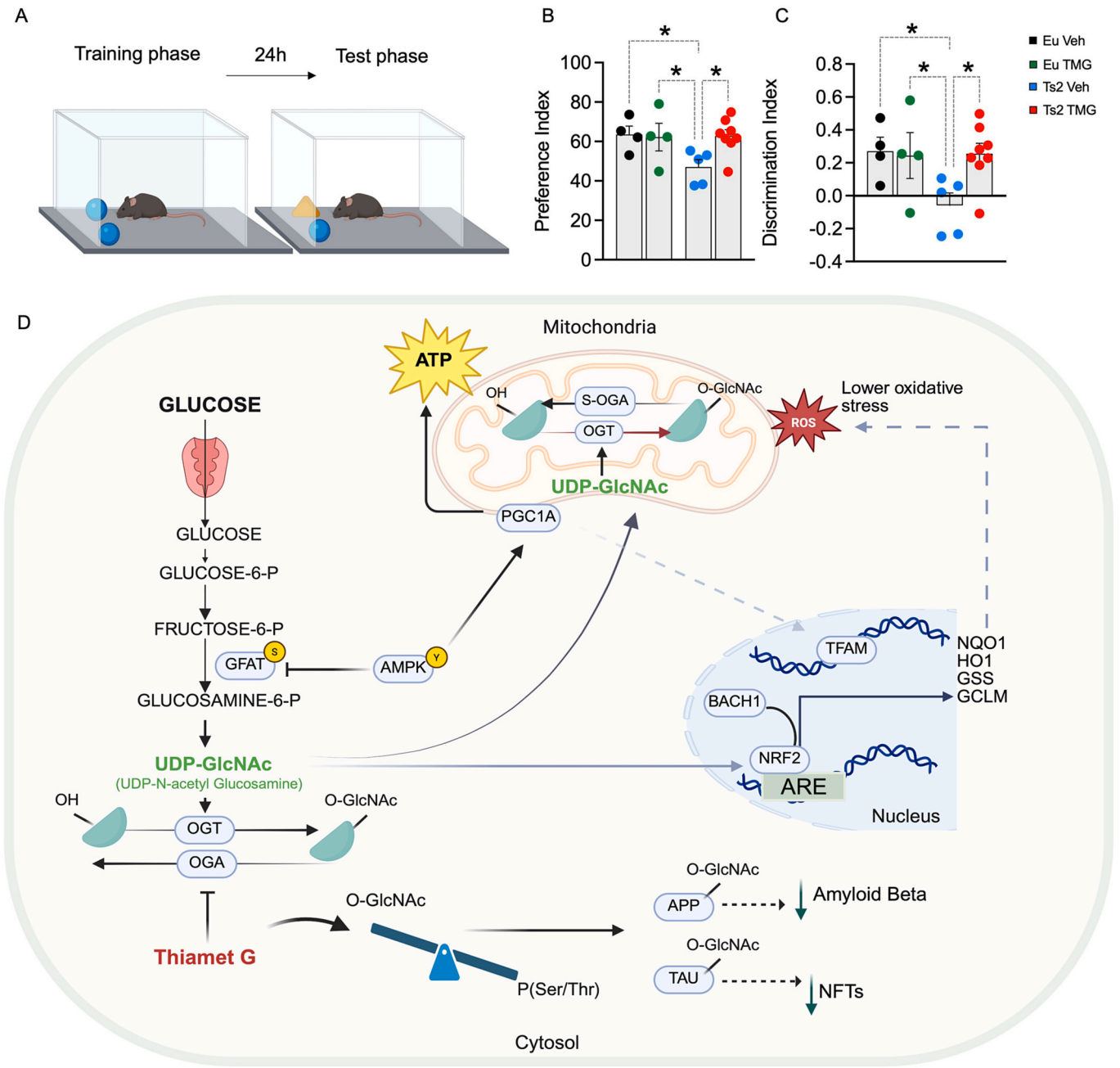

Fig. 10. Intranasal TMG administration improve recognition memory: **Putative scenario of molecular mechanism involving, APP, Tau, stress responses and mitochondrial activity amelioration. (A)** Scheme of the novel object recognition test. **(B)** Preference index and **(C)** Discrimination index. Data are presented as means ± SEM. Statistical significance was determined using One-way ANOVA with Fisher's LSD test. **(D)** The schematic illustrates the metabolic and molecular pathways linking the HBP and O-GlcNAcylation with mitochondrial function and protein homeostasis. Glucose is metabolized into UDP-GlcNAc through the HBP, with GFAT as a key enzyme regulated by AMPK phosphorylation. UDP-GlcNAc serves as the substrate for OGT, which facilitates protein O-GlcNAcylation, counterbalanced by OGA. TMG, an OGA inhibitor, enhances O-GlcNAcylation in Ts2 mice by the modulation of OGA activity, thereby influencing cellular energy metabolism, mitochondrial function, and protein stability. In mitochondria, UDP-GlcNAc is utilized by OGT, which O-GlcNAcylates specific mitochondrial proteins. S-OGA regulates mitochondrial activity and O-GlcNAc cycling, impacting the expression of key mitochondrial transcription factors such as PGC1A and TFAM. These factors enhance mitochondrial biogenesis and ATP synthesis. In addition, TMG stimulates NRF2 antioxidant pathway and ER-stress responses promoting the reduction of protein oxidative damage. The increase in O-GlcNAcylation following TMG treatment is counterbalanced by a decrease in total protein phosphorylation. This interplay is observed for APP and Tau and may leads to a reduction in the formation of NFT and Aβ, mitigating pathological processes associated with the development of AD in DS individuals. Created with Biorender.com.

metabolic triggers of reduced O-GlcNAc levels. However, the underlying molecular mechanisms that position O-GlcNAc as a mediator between nutrient availability, pathological signatures and neuronal function are still under investigation. Within this context, proteomics analysis allows the identification of proteins and pathways whose O-GlcNAc modulation is associated with pathological mechanisms. Previous proteomics studies aided in identifying defective pathways common to DS and AD [69] and demonstrated altered O-GlcNAc levels of proteins associated with neuronal structure, clearance of toxic aggregate and energy metabolism [17,66,70]. Recent multi-omics data by Slawson laboratory highlighted the importance of O-GlcNAc homeostasis in the regulation of mTOR/AMPK axis, proteasome functions and amino acids

metabolism [71]. These data agree with our current and previous findings that position AMPK as a central regulatory hub of the O-GlcNAcylation process, despite we did not find changes for mTOR signalling [18]. Remarkably, our results support the notion that the efficacy of TMG is linked to its ability to restore O-GlcNAc levels in proteins critical for pathways associated with brain architecture, ROS detoxification, and bioenergetics. Notably, our proteomics analysis highlights the modulation of proteins involved in brain energy-producing processes, including OXPHOS (ATP synthase F1 subunit alpha and beta and ubiquinol-cytochrome c reductase core protein 1), as a primary effect of TMG treatment in DS mice. Accordingly, network analysis reveals a complex interplay between APP, Tau and mitochondrial components, including elements of the ETC, and BDNF (Fig. 4C and D). Moreover, we also observed that increased O-GlcNAc levels of proteins regulating mitochondrial proteostasis, including HSP60. These data underscore TMG ability to address metabolic, regulatory and structural deficits in DS neuropathology. O-GlcNAc emerges as a crucial regulator of mitochondrial function, with both OGT and OGA found to localize within mitochondria [72]. Remarkably, many proteins controlling mitochondrial energy metabolism, oxidative stress, morphology, and dynamics are regulated by O-GlcNAcylation [55]. Reduced O-GlcNAcylation observed in *in vitro* models of AD promote mitochondrial abnormalities and cell death induction [67]. Additionally, the increase of Aβ levels were shown to reduce ATPase activity by affecting the O-GlcNAcylation of the ATP synthase subunit α (ATP5A) [73]. Short-term inhibition of OGA in rats has been shown to enhance oxygen consumption in isolated mitochondria [70], whereas prolonged elevation of O-GlcNAcylation, accompanied by increased OGA expression, has been found to influence mitochondrial function and reprogram the transcriptome [54]. In neurons, O-GlcNAcylation provides a fuel-dependent feedforward control mechanism to optimize mitochondrial performance based on neuronal activity, thereby coupling neuronal metabolism to mitochondrial bioenergetics [74]. Nevertheless, increased O-GlcNAc stimulates mitophagy thus improving mitochondrial turnover and activity [49], while OGT regulates the proteasome/mitochondrial axis in a manner that maintains mitochondrial fitness and cell viability [75]. Our data confirm an increase of mitochondrial O-GlcNAc levels in the DS mice administered with TMG, which is associated with the modulation of mitochondrial OGT and OGA levels. This effect is further confirmed by proteomics data that show the enrichment of over-*O*-GlcNAcylated proteins within the mitochondria following TMG treatment, potentially linked to the observed selective inhibition of sOGA. Moreover, the increased expression and activity of NDUFB8 (Complex I) subunit observed in treated animals corroborate the improvements of mitochondrial functionality and its role in ameliorating AD-related bioenergetics defects. Additionally, the rescue of mitochondrial O-GlcNAc appear to be related with increased biogenesis, as suggested by TFAM expression levels. Improved mitochondrial function may also promote reduced ROS leakage and the observed reduction of protein oxidative damage. Nevertheless, proteomics and biochemical results also support a profound association between O-GlcNAc cycle and redox responses, as described before [53]. Indeed, the analysis of the NRF2 antioxidant response support a regulatory role for O-GlcNAc levels, whose increase through TMG treatment promote NRF2 expression, nuclear translocation and transcriptional activity. As well, our findings confirm a link between O-GlcNAc and the induction of the ER-resident protein ATF4, as described by pathways analyses and previously observed [49]. In this scenario, our results support that increased O-GlcNAcylation, exerted by TMG administration, might act as homeostatic regulation able to restore molecular mechanisms affected by mitochondrial energetic crisis, redox imbalance, neuronal and synaptic degeneration. Notably, while our findings suggest a link between O-GlcNAc modulation and improvements in mitochondrial and redox function, the causal relationship remains indirect and would require further investigation. Nonetheless, O-GlcNAc levels by regulating APP and Tau post-translational modification may reduce the formation of toxic aggregates [18] and their synergistic effects in accelerating neuronal damage and the progression of early onset AD-like pathology [19,22,76]. Studies on murine models of AD have shown that restoring brain O-GlcNAc levels reduce the amyloidogenic cleavage of APP, promotes the removal of Aβ toxic aggregates and lowers pathological Tau levels [19,63,77–79]. In cell cultures treated with OGA inhibitors or OGA siRNAs, an increase in non-amyloidogenic sAPPα and a decrease in Aβ secretion were observed [78]. Accordingly, increased Tau O-GlcNAcylation maintained the protein in a soluble and non-toxic form preventing its aggregation [80]. Furthermore, literature studies report that cytoskeletal proteins appear to be particularly responsive to O-GlcNAc modulation, likely due to their functional dependence on phosphorylation-based regulation [12,81]. Studies from our laboratory embrace the hypothesis that OGA inhibition restore the balance between O-GlcNAcylation and phosphorylation of APP and Tau, thereby ameliorating the formation of pathological hallmarks in DS individuals and in normal population [14,18,77,78,82]. Indeed, we demonstrate that the administration of TMG in DS mice promote the mitigation of AD signatures as observed for decreased soluble Aβ levels. In addition, degree of colocalization between pAPP T668 and O-GlcNAc, and between pTau AT8 and O-GlcNAc in Ts2 mice following TMG treatment suggests a biologically relevant shift consistent with current models describing a competitive rather than cooperative interaction between phosphorylation and O-GlcNAcylation [12]. In particular, data on Tau protein support the hypothesis that enhancing O-GlcNAc levels disrupts phosphorylation at specific sites, aligning with prior findings that O-GlcNAcylation can antagonize its pathological phosphorylation and stabilize Tau in a less aggregated, functionally regulated state [82,83].

In this scenario, the previously described amelioration of mitochondrial bioenergetic and the homeostatic regulation of APP and Tau PTMs are closely linked with the observed significant improvement in recognition memory, although spatial memory remains unaffected.

5. Conclusions

Overall, the present study demonstrates that a short-term treatment with intranasal TMG increases O-GlcNAc levels in the cortex and improves recognition memory in Ts2 mice. Cognitive improvement associates with changes in APP and Tau phosphorylation and with increased O-GlcNAc levels of proteins involved in pathways critical for the development of AD-like signatures. However, our findings extend TMG efficacy beyond APP and Tau amelioration by showing the amendment of cellular mechanisms related to neuronal architecture, synaptic plasticity, stress and redox responses and energy production (Fig. 9D). Notably, the enhancement of mitochondrial activity emerges as a particularly immediate and impactful mechanism, which we propose plays a central role in regulating brain physiology and underlies the observed improvement in recognition memory.

Based on these findings, we can support the notion that dysregulated O-GlcNAcylation along with mitochondrial dysfunction, and with increased Aβ and Tau aggregation may contribute to a self-perpetuating cycle that accelerates the progression of AD-like characters in DS. It is tempting to suggest that by solely targeting OGA activity TMG may halt this cycle and promote cognitive enhancements, thus mitigating mitochondrial defects, boosting stress responses, reducing oxidative stress, and restoring APP and Tau homeostasis. While ongoing clinical trials are currently evaluating TMG's safety and efficacy in humans, our findings remark its promise as a therapeutic strategy against AD-like neurodegeneration, benefiting not only individuals with DS but also the general population.

CRediT authorship contribution statement

Chiara Lanzillotta: Writing – review & editing, Writing – original draft, Visualization, Validation, Supervision, Software, Methodology, Investigation, Formal analysis, Data curation. **Francesca Prestia:**

Writing – original draft, Visualization, Validation, Software, Methodology, Investigation, Formal analysis, Data curation. **Viviana Greco:** Software, Investigation, Formal analysis, Data curation. **Federica Iavarone:** Validation, Formal analysis, Data curation. **Federica Cordella:** Visualization, Validation, Investigation, Data curation. **Chiara Sette:** Methodology, Investigation, Formal analysis. **Elena Forte:** Writing – review & editing, Methodology, Formal analysis. **Antonella Tramutola:** Writing – review & editing, Methodology, Investigation, Data curation. **Simona Lanzillotta:** Investigation, Formal analysis. **Tommaso Cassano:** Writing – review & editing, Methodology, Funding acquisition, Conceptualization. **Silvia Di Angelantonio:** Writing – review & editing, Methodology, Data curation. **Andrea Urbani:** Writing – review & editing, Supervision, Methodology, Data curation. **Eugenio Barone:** Writing – review & editing, Supervision, Resources, Data curation. **Marzia Perluigi:** Writing – review & editing, Supervision, Resources, Methodology, Data curation. **Fabio Di Domenico:** Writing – review & editing, Writing – original draft, Visualization, Supervision, Software, Resources, Project administration, Methodology, Investigation, Funding acquisition, Data curation, Conceptualization.

Fundings

This work was supported in part by a Fondi Ateneo grant funded by Sapienza University n. RG12117A75C98BE3 (to M.P.), and n. RM12117A2EC1C9E4, RM11916B78D5711A, and RG1181642744 DF59 (to F.D.D.); by the Institute Pasteur-Fondazione Cenci Bolognetti "2022-23 Anna Tramontano" (to M.P.); by the Ministry of University and Research (MUR) n.2022KP5LKS (to F.D.D.); by the Jerome Lejeune Foundation Grant #2280 –-2023b (to F.D.D.); by MUR PRIN 2022 (CUP: 2022CFP7RF, to SDA); by D-Tails-IIT Joint Lab (to SDA, YG); by the Regione Lazio FSE 2014–2020 (19036AP000000019 and A0112E0073) grants (to SDA). The research leading to these results has received funding from the European Union - NextGenerationEU through the Italian Ministry of University and Research under PNRR - M4C2-I1.3 Project PE_00000019 ″HEAL ITALIA" CUP: D73C22001230006 (to T. C.). The views and opinions expressed are those of the authors only and do not necessarily reflect those of the European Union or the European Commission. Neither the European Union nor the European Commission can be held responsible for them.

Declaration of competing interest

Silvia Di Angelantonio is a scientific advisor of D-Tails s.r.l. The funders had no role in the design of the study; in the collection, analysis, or interpretation of data; in the writing of the manuscript; or in the decision to publish the results.

All the other authors declare no competing interest.

Acknowledgements

The authors wish to thank the Center for Life Nano and Neuroscience Imaging Facility, Istituto Italiano di Tecnologia.

Appendix A. Supplementary data

Supplementary data to this article can be found online at https://doi.org/10.1016/j.redox.2025.103769.

Abbreviations

2-DE	2-dimensional electrophoresis
3-NT	3-nitrotyrosine
Aβ	Amyloid beta
AD	Alzheimer disease
AMPK	AMP-activated protein kinase
APP	Amyloid precursor protein
ATP5A	ATP synthase subunit α
BGC	Biological gene count
DEA	Diethanolamine
DI	Discrimination index
DS	Down syndrome
ER	Endoplasmic reticulum
Eu	Euploid
FDR	False discovery rate
GCLM	Glutamate-cysteine ligase modifier subunit
GFAT1	Glutamine:fructose-6-phosphate aminotransferase 1
GO	Gene onthology
GSS	Glutathione synthetase
O-GlcNAc	O-linked N-acetylglucosamine
HBP	Hexosamine biosynthetic pathway
HO-1	Heme oxygenase 1
KEGG	Kyoto encyclopedia of genes and genomes
MS	Mass spectrometry
NA	Novel arm
NFT	Neurofibrillary tangles
NOR	Novel Object Recognition
NQO1	NAD quinone oxidoreductase 1
OGA	(protein)-3-*O*-(N-acetyl-D-glucosaminyl)-L-serine/threonine N-acetylglucosaminyl hydrolase
OGC	Observed gene count
OXPHOS	Oxidative phosphorylation
OGT	Protein O-GlcNAc transferase
PC	Protein carbonyl
PI	Preference index
PTM	Post translational modification
ROS	Reactive oxygen species
SDS PAGE	Sodium dodecyl sulphate polyacrylamide gel electrophoresis
Ser	Serine
STR	Strength
Thr	Threonine
TMG	Thiamet G
Ts2	Ts2Cje
UDP-GlcNAc	Uridine diphosphate N-acetylglucosamine
Veh	Vehicle
WB	Western blot

Data availability

Data will be made available on request.

References

[1] I. Akan, S. Olivier-Van Stichelen, M.R. Bond, J.A. Hanover, Nutrient-driven O-GlcNAc in proteostasis and neurodegeneration, J. Neurochem. 144 (1) (2018) 7–34, https://doi.org/10.1111/jnc.14242.

[2] J. Flax, H.M. Wilkins, R. Miller, S. Griffith, G.K. Cork, A. Qiang, J. Thompson, R. H. Swerdlow, C. Slawson, OGA inhibition alters energetics and nutrient sensing in Alzheimer's Disease cytoplasmic hybrids, J. Alzheimers Dis. 78 (4) (2020) 1743–1753, https://doi.org/10.3233/JAD-200996.

[3] S. Hardiville, G.W. Hart, Nutrient regulation of signaling, transcription, and cell physiology by O-GlcNAcylation, Cell Metab. 20 (2) (2014) 208–213, https://doi.org/10.1016/j.cmet.2014.07.014.

[4] K.R. Harwood, J.A. Hanover, Nutrient-driven O-GlcNAc cycling - think globally but act locally, J. Cell Sci. 127 (Pt 9) (2014) 1857–1867, https://doi.org/10.1242/jcs.113233.

[5] X. Yang, K. Qian, Protein O-GlcNAcylation: emerging mechanisms and functions, Nat. Rev. Mol. Cell Biol. 18 (7) (2017) 452–465, https://doi.org/10.1038/nrm.2017.22.

[6] G.W. Hart, Y. Akimoto, The O-GlcNAc modification, in: nd, A. Varki, R. D. Cummings, J.D. Esko, H.H. Freeze, P. Stanley, C.R. Bertozzi, G.W. Hart, M. E. Etzler (Eds.), Essentials of Glycobiology, Cold Spring Harbor (NY), 2009.

[7] C.M. West, C. Slawson, N.E. Zachara, G.W. Hart, Nucleocytoplasmic glycosylation, in: A. Varki, R.D. Cummings, J.D. Esko, P. Stanley, G.W. Hart, M. Aebi, D. Mohnen, T. Kinoshita, N.H. Packer, J.H. Prestegard, R.L. Schnaar, P.H. Seeberger (Eds.), Essentials of Glycobiology, Cold Spring Harbor (NY), 2022, pp. 233–250.

[8] H.B. Ruan, J.P. Singh, M.D. Li, J. Wu, X. Yang, Cracking the O-GlcNAc code in metabolism, Trends Endocrinol. Metabol. 24 (6) (2013) 301–309, https://doi.org/10.1016/j.tem.2013.02.002.

[9] C. Slawson, New ways of thinking about old things: the role of O-GlcNAc in cellular metabolism, J. Bioenerg. Biomembr. 50 (3) (2018) 153–154, https://doi.org/10.1007/s10863-018-9762-z.

[10] C. Butkinaree, K. Park, G.W. Hart, O-linked beta-N-acetylglucosamine (O-GlcNAc): extensive crosstalk with phosphorylation to regulate signaling and transcription in response to nutrients and stress, Biochim. Biophys. Acta 1800 (2) (2010) 96–106, https://doi.org/10.1016/j.bbagen.2009.07.018.

[11] C. Slawson, G.W. Hart, Dynamic interplay between O-GlcNAc and O-phosphate: the sweet side of protein regulation, Curr. Opin. Struct. Biol. 13 (5) (2003) 631–636, https://doi.org/10.1016/j.sbi.2003.08.003.

[12] Z. Wang, M. Gucek, G.W. Hart, Cross-talk between GlcNAcylation and phosphorylation: site-specific phosphorylation dynamics in response to globally elevated O-GlcNAc, Proc. Natl. Acad. Sci. U. S. A. 105 (37) (2008) 13793–13798, https://doi.org/10.1073/pnas.0806216105.

[13] J.M. Bartolome-Nebreda, A.A. Trabanco, A.I. Velter, P. Buijnsters, O-GlcNAcase inhibitors as potential therapeutics for the treatment of Alzheimer's disease and related tauopathies: analysis of the patent literature, Expert Opin. Ther. Pat. 31 (12) (2021) 1117–1154, https://doi.org/10.1080/13543776.2021.1947242.

[14] E. Gatta, T. Lefebvre, S. Gaetani, M. dos Santos, J. Marrocco, A.M. Mir, T. Cassano, S. Maccari, F. Nicoletti, J. Mairesse, Evidence for an imbalance between tau O-GlcNAcylation and phosphorylation in the hippocampus of a mouse model of Alzheimer's disease, Pharmacol. Res. 105 (2016) 186–197, https://doi.org/10.1016/j.phrs.2016.01.006.

[15] C.X. Gong, F. Liu, I. Grundke-Iqbal, K. Iqbal, Impaired brain glucose metabolism leads to Alzheimer neurofibrillary degeneration through a decrease in tau O-GlcNAcylation, J. Alzheimers Dis. 9 (1) (2006) 1–12, https://doi.org/10.3233/jad-2006-9101.

[16] F. Liu, J. Shi, H. Tanimukai, J. Gu, J. Gu, I. Grundke-Iqbal, K. Iqbal, C.X. Gong, Reduced O-GlcNAcylation links lower brain glucose metabolism and tau pathology in Alzheimer's disease, Brain 132 (Pt 7) (2009) 1820–1832, https://doi.org/10.1093/brain/awp099.

[17] A. Tramutola, N. Sharma, E. Barone, C. Lanzillotta, A. Castellani, F. Iavarone, F. Vincenzoni, M. Castagnola, D.A. Butterfield, S. Gaetani, T. Cassano, M. Perluigi, F. Di Domenico, Proteomic identification of altered protein O-GlcNAcylation in a triple transgenic mouse model of Alzheimer's disease, Biochim. Biophys. Acta Mol. Basis Dis. 1864 (10) (2018) 3309–3321, https://doi.org/10.1016/j.bbadis.2018.07.017.

[18] I. Zuliani, C. Lanzillotta, A. Tramutola, A. Francioso, S. Pagnotta, E. Barone, M. Perluigi, F. Di Domenico, The dysregulation of OGT/OGA cycle mediates Tau and APP neuropathology in Down syndrome, Neurotherapeutics (2020), https://doi.org/10.1007/s13311-020-00978-4.

[19] E. Head, A.M. Helman, D. Powell, F.A. Schmitt, Down syndrome, beta-amyloid and neuroimaging, Free Radic. Biol. Med. 114 (2018) 102–109, https://doi.org/10.1016/j.freeradbiomed.2017.09.013.

[20] E. Head, I.T. Lott, D.M. Wilcock, C.A. Lemere, Aging in Down syndrome and the development of Alzheimer's Disease neuropathology, Curr. Alzheimer Res. 13 (1) (2016) 18–29, https://doi.org/10.2174/1567205012666151020114607.

[21] F.K. Wiseman, T. Al-Janabi, J. Hardy, A. Karmiloff-Smith, D. Nizetic, V. L. Tybulewicz, E.M. Fisher, A. Strydom, A genetic cause of Alzheimer disease: mechanistic insights from Down syndrome, Nat. Rev. Neurosci. 16 (9) (2015) 564–574, https://doi.org/10.1038/nrn3983.

[22] S.E. Antonarakis, B.G. Skotko, M.S. Rafii, A. Strydom, S.E. Pape, D.W. Bianchi, S. L. Sherman, R.H. Reeves, Down syndrome, Nat. Rev. Dis. Primers 6 (1) (2020) 9, https://doi.org/10.1038/s41572-019-0143-7.

[23] E.D. Hamlett, H.A. Boger, A. Ledreux, C.M. Kelley, E.J. Mufson, M.F. Falangola, D. N. Guilfoyle, R.A. Nixon, D. Patterson, N. Duval, A.C. Granholm, Cognitive impairment, neuroimaging, and alzheimer neuropathology in mouse models of Down syndrome, Curr. Alzheimer Res. 13 (1) (2016) 35–52, https://doi.org/10.2174/1567205012666150921095505.

[24] C. Lanzillotta, F. Di Domenico, Stress responses in Down syndrome neurodegeneration: state of the art and therapeutic molecules, Biomolecules 11 (2) (2021), https://doi.org/10.3390/biom11020266.

[25] C. Lanzillotta, A. Tramutola, G. Di Giacomo, F. Marini, D.A. Butterfield, F. Di Domenico, M. Perluigi, E. Barone, Insulin resistance, oxidative stress and mitochondrial defects in Ts65dn mice brain: a harmful synergistic path in Down syndrome, Free Radic. Biol. Med. 165 (2021) 152–170, https://doi.org/10.1016/j.freeradbiomed.2021.01.042.

[26] A. Tramutola, C. Lanzillotta, F. Di Domenico, E. Head, D.A. Butterfield, M. Perluigi, E. Barone, Brain insulin resistance triggers early onset Alzheimer disease in Down syndrome, Neurobiol. Dis. 137 (2020) 104772, https://doi.org/10.1016/j.nbd.2020.104772.

[27] M. Dierssen, M. Fructuoso, M. Martinez de Lagran, M. Perluigi, E. Barone, Down syndrome is a metabolic disease: altered insulin signaling mediates peripheral and brain dysfunctions, Front. Neurosci. 14 (2020) 670, https://doi.org/10.3389/fnins.2020.00670.

[28] F. Di Domenico, C. Lanzillotta, A. Tramutola, Therapeutic potential of rescuing protein O-GlcNAcylation in tau-related pathologies, Expert Rev. Neurother. 19 (1) (2019) 1–3, https://doi.org/10.1080/14737175.2019.1540932.

[29] I. Zuliani, C. Lanzillotta, A. Tramutola, E. Barone, M. Perluigi, S. Rinaldo, A. Paone, F. Cutruzzola, F. Bellanti, M. Spinelli, F. Natale, S. Fusco, C. Grassi, F. Di Domenico, High-fat diet leads to reduced protein O-GlcNAcylation and mitochondrial defects promoting the development of Alzheimer's Disease signatures, Int. J. Mol. Sci. 22 (7) (2021), https://doi.org/10.3390/ijms22073746.

[30] A.J. Villar, P.V. Belichenko, A.M. Gillespie, H.M. Kozy, W.C. Mobley, C.J. Epstein, Identification and characterization of a new Down syndrome model, Ts[Rb (12.1716)]2Cje, resulting from a spontaneous Robertsonian fusion between T(171) 65Dn and mouse chromosome 12, Mamm. Genome 16 (2) (2005) 79–90, https://doi.org/10.1007/s00335-004-2428-7.

[31] L.G. Reinholdt, Y. Ding, G.J. Gilbert, A. Czechanski, J.P. Solzak, R.J. Roper, M. T. Johnson, L.R. Donahue, C. Lutz, M.T. Davisson, Molecular characterization of the translocation breakpoints in the Down syndrome mouse model Ts65Dn, Mamm. Genome 22 (11–12) (2011) 685–691, https://doi.org/10.1007/s00335-011-9357-z.

[32] Y. Yu, L. Zhang, X. Li, X. Run, Z. Liang, Y. Li, Y. Liu, M.H. Lee, I. Grundke-Iqbal, K. Iqbal, D.J. Vocadlo, F. Liu, C.X. Gong, Differential effects of an O-GlcNAcase inhibitor on tau phosphorylation, PLoS One 7 (4) (2012) e35277, https://doi.org/10.1371/journal.pone.0035277.

[33] M. Antunes, G. Biala, The novel object recognition memory: neurobiology, test procedure, and its modifications, Cogn. Process. 13 (2) (2012) 93–110, https://doi.org/10.1007/s10339-011-0430-z.

[34] A. Ennaceur, One-trial object recognition in rats and mice: methodological and theoretical issues, Behav. Brain Res. 215 (2) (2010) 244–254, https://doi.org/10.1016/j.bbr.2009.12.036.

[35] A.K. Kraeuter, P.C. Guest, Z. Sarnyai, The Y-Maze for assessment of spatial working and reference memory in mice, Methods Mol. Biol. 1916 (2019) 105–111, https://doi.org/10.1007/978-1-4939-8994-2_10.

[36] I. Dimauro, T. Pearson, D. Caporossi, M.J. Jackson, A simple protocol for the subcellular fractionation of skeletal muscle cells and tissue, BMC Res. Notes 5 (2012) 513, https://doi.org/10.1186/1756-0500-5-513.

[37] K.J. Livak, T.D. Schmittgen, Analysis of relative gene expression data using real-time quantitative PCR and the 2(-Delta Delta C(T)) method, Methods 25 (4) (2001) 402–408, https://doi.org/10.1006/meth.2001.1262.

[38] N.E. Zachara, K. Vosseller, G.W. Hart, Detection and analysis of proteins modified by O-linked N-acetylglucosamine, Curr. Protoc. Mol. Biol. Chapter 17 (2011), https://doi.org/10.1002/0471142727.mb1706s95. Unit 17 6.

[39] D. Valenti, L. de Bari, B. De Filippis, L. Ricceri, R.A. Vacca, Preservation of mitochondrial functional integrity in mitochondria isolated from small cryopreserved mouse brain areas, Anal. Biochem. 444 (2014) 25–31, https://doi.org/10.1016/j.ab.2013.08.030.

[40] M. Milacic, D. Beavers, P. Conley, C. Gong, M. Gillespie, J. Griss, R. Haw, B. Jassal, L. Matthews, B. May, R. Petryszak, E. Ragueneau, K. Rothfels, C. Sevilla, V. Shamovsky, R. Stephan, K. Tiwari, T. Varusai, J. Weiser, A. Wright, G. Wu, L. Stein, H. Hermjakob, P. D'Eustachio, The Reactome Pathway Knowledgebase 2024, Nucleic Acids Res. 52 (D1) (2024) D672–D678, https://doi.org/10.1093/nar/gkad1025.

[41] D. Szklarczyk, R. Kirsch, M. Koutrouli, K. Nastou, F. Mehryary, R. Hachilif, A. L. Gable, T. Fang, N.T. Doncheva, S. Pyysalo, P. Bork, L.J. Jensen, C. von Mering, The STRING database in 2023: protein-protein association networks and functional enrichment analyses for any sequenced genome of interest, Nucleic Acids Res. 51 (D1) (2023) D638–D646, https://doi.org/10.1093/nar/gkac1000.

[42] A. Tramutola, C. Lanzillotta, E. Barone, A. Arena, I. Zuliani, L. Mosca, C. Blarzino, D.A. Butterfield, M. Perluigi, F. Di Domenico, Intranasal rapamycin ameliorates alzheimer-like cognitive decline in a mouse model of Down syndrome, Transl. Neurodegener. 7 (2018) 28, https://doi.org/10.1186/s40035-018-0133-9.

[43] M.R. Pratt, D.J. Vocadlo, Understanding and exploiting the roles of O-GlcNAc in neurodegenerative diseases, J. Biol. Chem. 299 (12) (2023) 105411, https://doi.org/10.1016/j.jbc.2023.105411.

[44] T.J. Gross, E. Doran, A.K. Cheema, E. Head, I.T. Lott, M. Mapstone, Plasma metabolites related to cellular energy metabolism are altered in adults with Down syndrome and Alzheimer's disease, Dev. Neurobiol. 79 (7) (2019) 622–638, https://doi.org/10.1002/dneu.22716.

[45] M. Morgenstern, C.D. Peikert, P. Lubbert, I. Suppanz, C. Klemm, O. Alka, C. Steiert, N. Naumenko, A. Schendzielorz, L. Melchionda, W.W.D. Muhlhauser, B. Knapp, J. D. Busch, S.B. Stiller, S. Dannenmaier, C. Lindau, M. Licheva, C. Eickhorst, R. Galbusera, R.M. Zerbes, M.T. Ryan, C. Kraft, V. Kozjak-Pavlovic, F. Drepper, S. Dennerlein, S. Oeljeklaus, N. Pfanner, N. Wiedemann, B. Warscheid, Quantitative high-confidence human mitochondrial proteome and its dynamics in cellular context, Cell Metab. 33 (12) (2021) 2464–2483 e18, https://doi.org/10.1016/j.cmet.2021.11.001.

[46] K.L. Tan, H.C. Lee, P.S. Cheah, K.H. Ling, Mitochondrial dysfunction in Down Syndrome: from pathology to therapy, Neuroscience 511 (2023) 1–12, https://doi.org/10.1016/j.neuroscience.2022.12.003.

[47] D. Valenti, N. Braidy, D. De Rasmo, A. Signorile, L. Rossi, A.G. Atanasov, M. Volpicella, A. Henrion-Caude, S.M. Nabavi, R.A. Vacca, Mitochondria as pharmacological targets in Down syndrome, Free Radic. Biol. Med. 114 (2018) 69–83, https://doi.org/10.1016/j.freeradbiomed.2017.08.014.

[48] J. Dontaine, A. Bouali, F. Daussin, L. Bultot, D. Vertommen, M. Martin, R. Rathagirishnan, A. Cuillerier, S. Horman, C. Beauloye, L. Gatto, B. Lauzier, L. Bertrand, Y. Burelle, The intra-mitochondrial O-GlcNAcylation system rapidly modulates OXPHOS function and ROS release in the heart, Commun. Biol. 5 (1) (2022) 349, https://doi.org/10.1038/s42003-022-03282-3.

[49] I.M. Alghusen, M.S. Carman, H. Wilkins, S.J. Ephrame, A. Qiang, W.B. Dias, H. Fedosyuk, A.R. Denson, R.H. Swerdlow, C. Slawson, O-GlcNAc regulates the mitochondrial integrated stress response by regulating ATF4, Front. Aging Neurosci. 15 (2023) 1326127, https://doi.org/10.3389/fnagi.2023.1326127.

[50] T.S. Pinho, D.M. Verde, S.C. Correia, S.M. Cardoso, P.I. Moreira, O-GlcNAcylation and neuronal energy status: implications for Alzheimer's disease, Ageing Res. Rev. 46 (2018) 32–41, https://doi.org/10.1016/j.arr.2018.05.003.

[51] Z.W. Tan, G. Fei, J.A. Paulo, S. Bellaousov, S.E.S. Martin, D.Y. Duveau, C. J. Thomas, S.P. Gygi, P.L. Boutz, S. Walker, O-GlcNAc regulates gene expression by controlling detained intron splicing, Nucleic Acids Res. 48 (10) (2020) 5656–5669, https://doi.org/10.1093/nar/gkaa263.
[52] P. Pagesy, A. Bouaboud, Z. Feng, P. Hulin, T. Issad, Short O-GlcNAcase is targeted to the Mitochondria and regulates mitochondrial reactive oxygen species level, Cells 11 (11) (2022), https://doi.org/10.3390/cells11111827.
[53] P.H. Chen, J.T. Chi, M. Boyce, Functional crosstalk among oxidative stress and O-GlcNAc signaling pathways, Glycobiology 28 (8) (2018) 556–564, https://doi.org/10.1093/glycob/cwy027.
[54] E.P. Tan, S.R. McGreal, S. Graw, R. Tessman, S.J. Koppel, P. Dhakal, Z. Zhang, M. Machacek, N.E. Zachara, D.C. Koestler, K.R. Peterson, J.P. Thyfault, R. H. Swerdlow, P. Krishnamurthy, L. DiTacchio, U. Apte, C. Slawson, Sustained O-GlcNAcylation reprograms mitochondrial function to regulate energy metabolism, J. Biol. Chem. 292 (36) (2017) 14940–14962, https://doi.org/10.1074/jbc.M117.797944.
[55] C.W. Huang, N.C. Rust, H.F. Wu, G.W. Hart, Altered O-GlcNAcylation and mitochondrial dysfunction, a molecular link between brain glucose dysregulation and sporadic Alzheimer's disease, Neural Regen. Res. 18 (4) (2023) 779–783, https://doi.org/10.4103/1673-5374.354515.
[56] J. Arambasic, M. Mihailovic, A. Uskokovic, S. Dinic, N. Grdovic, J. Markovic, G. Poznanovic, D. Bajec, M. Vidakovic, Alpha-lipoic acid upregulates antioxidant enzyme gene expression and enzymatic activity in diabetic rat kidneys through an O-GlcNAc-dependent mechanism, Eur. J. Nutr. 52 (5) (2013) 1461–1473, https://doi.org/10.1007/s00394-012-0452-z.
[57] B. Buttari, A. Tramutola, A.I. Rojo, N. Chondrogianni, S. Saha, A. Berry, L. Giona, J. P. Miranda, E. Profumo, S. Davinelli, A. Daiber, A. Cuadrado, F. Di Domenico, Proteostasis decline and redox imbalance in age-related diseases: the therapeutic potential of NRF2, Biomolecules 15 (1) (2025), https://doi.org/10.3390/biom15010113.
[58] L. Yang, H. Tang, J. Wang, D. Xu, R. Xuan, S. Xie, P. Xu, X. Li, O-GlcNAcylation attenuates ischemia-reperfusion-induced pulmonary epithelial cell ferroptosis via the Nrf2/G6PDH pathway, BMC Biol. 23 (1) (2025) 32, https://doi.org/10.1186/s12915-025-02126-w.
[59] M. Margallo-Lana, C.M. Morris, A.M. Gibson, A.L. Tan, D.W. Kay, S.P. Tyrer, B. P. Moore, C.G. Ballard, Influence of the amyloid precursor protein locus on dementia in Down syndrome, Neurology 62 (11) (2004) 1996–1998, https://doi.org/10.1212/01.wnl.0000129275.13169.be.
[60] D.A. Butterfield, F. Di Domenico, A.M. Swomley, E. Head, M. Perluigi, Redox proteomics analysis to decipher the neurobiology of Alzheimer-like neurodegeneration: overlaps in Down's syndrome and Alzheimer's disease brain, Biochem. J. 463 (2) (2014) 177–189, https://doi.org/10.1042/BJ20140772.
[61] C. Farrell, P. Mumford, F.K. Wiseman, Rodent modeling of Alzheimer's Disease in Down syndrome: in vivo and ex vivo approaches, Front. Neurosci. 16 (2022) 909669, https://doi.org/10.3389/fnins.2022.909669.
[62] C. Lanzillotta, I. Zuliani, A. Tramutola, E. Barone, C. Blarzino, V. Folgiero, M. Caforio, D. Valentini, A. Villani, F. Locatelli, D.A. Butterfield, E. Head, M. Perluigi, J.F. Abisambra, F. Di Domenico, Chronic PERK induction promotes alzheimer-like neuropathology in Down syndrome: insights for therapeutic intervention, Prog. Neurobiol. 196 (2021) 101892, https://doi.org/10.1016/j.pneurobio.2020.101892.
[63] K.A. Chang, H.S. Kim, T.Y. Ha, J.W. Ha, K.Y. Shin, Y.H. Jeong, J.P. Lee, C.H. Park, S. Kim, T.K. Baik, Y.H. Suh, Phosphorylation of amyloid precursor protein (APP) at Thr668 regulates the nuclear translocation of the APP intracellular domain and induces neurodegeneration, Mol. Cell Biol. 26 (11) (2006) 4327–4338, https://doi.org/10.1128/MCB.02393-05.
[64] S. Egeback Arulf, R. Ziyue Zhou, B.E. Kirsebom, A. Jejcic, T. Fladby, B. Winblad, L. Tjernberg, S. Schedin-Weiss, Bisecting N-Acetylglucosamine correlates with Phospho-Tau181 in subjective cognitive decline but not in control cases, J. Alzheimers Dis. 100 (s1) (2024) S93–S101, https://doi.org/10.3233/JAD-240628.
[65] S. Valbuena, A. Garcia, W. Mazier, A.V. Paternain, J. Lerma, Unbalanced dendritic inhibition of CA1 neurons drives spatial-memory deficits in the Ts2Cje Down syndrome model, Nat. Commun. 10 (1) (2019) 4991, https://doi.org/10.1038/s41467-019-13004-9.
[66] R.A. Burt, I.M. Alghusen, S. John Ephrame, M.T. Villar, A. Artigues, C. Slawson, Mapping the O-GlcNAc modified proteome: applications for health and disease, Front. Mol. Biosci. 9 (2022) 920727, https://doi.org/10.3389/fmolb.2022.920727.
[67] T.S. Pinho, S.C. Correia, G. Perry, A.F. Ambrosio, P.I. Moreira, Diminished O-GlcNAcylation in Alzheimer's disease is strongly correlated with mitochondrial anomalies, Biochim. Biophys. Acta Mol. Basis Dis. 1865 (8) (2019) 2048–2059, https://doi.org/10.1016/j.bbadis.2018.10.037.
[68] S.A. Ansari, B.S. Emerald, The role of insulin resistance and protein O-GlcNAcylation in neurodegeneration, Front. Neurosci. 13 (2019) 473, https://doi.org/10.3389/fnins.2019.00473.
[69] M. Perluigi, F. Di Domenico, D.A. Buttterfield, Unraveling the complexity of neurodegeneration in brains of subjects with Down syndrome: insights from proteomics, Proteonomics Clin. Appl. 8 (1–2) (2014) 73–85, https://doi.org/10.1002/prca.201300066.
[70] J. Ma, T. Liu, A.C. Wei, P. Banerjee, B. O'Rourke, G.W. Hart, O-GlcNAcomic profiling identifies widespread O-Linked beta-N-Acetylglucosamine modification (O-GlcNAcylation) in oxidative phosphorylation system regulating cardiac mitochondrial function, J. Biol. Chem. 290 (49) (2015) 29141–29153, https://doi.org/10.1074/jbc.M115.691741.
[71] S.S. Boyd, D.R. Robarts, K. Nguyen, M. Villar, I.M. Alghusen, M. Kotulkar, A. Denson, H. Fedosyuk, S.A. Whelan, N.C.Y. Lee, J. Hanover, W.B. Dias, E.P. Tan, S.R. McGreal, A. Artigues, R.H. Swerdlow, J.A. Thompson, U. Apte, C. Slawson, Multi-omics after O-GlcNAc alteration identified cellular processes promoting aneuploidy after loss of O-GlcNAc transferase, Mol. Metabol. 90 (2024) 102060, https://doi.org/10.1016/j.molmet.2024.102060.
[72] P.S. Banerjee, J. Ma, G.W. Hart, Diabetes-associated dysregulation of O-GlcNAcylation in rat cardiac mitochondria, Proc. Natl. Acad. Sci. U. S. A. 112 (19) (2015) 6050–6055, https://doi.org/10.1073/pnas.1424017112.
[73] M.Y. Cha, H.J. Cho, C. Kim, Y.O. Jung, M.J. Kang, M.E. Murray, H.S. Hong, Y. J. Choi, H. Choi, D.K. Kim, H. Choi, J. Kim, D.W. Dickson, H.K. Song, J.W. Cho, E. C. Yi, J. Kim, S.M. Jin, I. Mook-Jung, Mitochondrial ATP synthase activity is impaired by suppressed O-GlcNAcylation in Alzheimer's disease, Hum. Mol. Genet. 24 (22) (2015) 6492–6504, https://doi.org/10.1093/hmg/ddv358.
[74] S.B. Yu, H. Wang, R.G. Sanchez, N.M. Carlson, K. Nguyen, A. Zhang, Z.D. Papich, A. A. Abushawish, Z. Whiddon, W. Matysik, J. Zhang, T.C. Whisenant, M. Ghassemian, J.N. Koberstein, M.L. Stewart, S.A. Myers, G. Pekkurnaz, Neuronal activity-driven O-GlcNAcylation promotes mitochondrial plasticity, Dev. Cell 59 (16) (2024) 2143–2157 e9, https://doi.org/10.1016/j.devcel.2024.05.008.
[75] X. Li, X. Yue, H. Sepulveda, R.A. Burt, D.A. Scott, A.C. S, A.M. S, A. Rao, OGT controls mammalian cell viability by regulating the proteasome/mTOR/mitochondrial axis, Proc. Natl. Acad. Sci. U. S. A. 120 (3) (2023) e2218332120, https://doi.org/10.1073/pnas.2218332120.
[76] I.T. Lott, E. Head, Dementia in Down syndrome: unique insights for Alzheimer disease research, Nat. Rev. Neurol. 15 (3) (2019) 135–147, https://doi.org/10.1038/s41582-018-0132-6.
[77] Y.S. Chun, O.H. Kwon, S. Chung, O-GlcNAcylation of amyloid-beta precursor protein at threonine 576 residue regulates trafficking and processing, Biochem. Biophys. Res. Commun. 490 (2) (2017) 486–491, https://doi.org/10.1016/j.bbrc.2017.06.067.
[78] K.T. Jacobsen, K. Iverfeldt, O-GlcNAcylation increases non-amyloidogenic processing of the amyloid-beta precursor protein (APP), Biochem. Biophys. Res. Commun. 404 (3) (2011) 882–886, https://doi.org/10.1016/j.bbrc.2010.12.080.
[79] C. Kim, D.W. Nam, S.Y. Park, H. Song, H.S. Hong, J.H. Boo, E.S. Jung, Y. Kim, J. Y. Baek, K.S. Kim, J.W. Cho, I. Mook-Jung, O-linked beta-N-acetylglucosaminidase inhibitor attenuates beta-amyloid plaque and rescues memory impairment, Neurobiol. Aging 34 (1) (2013) 275–285, https://doi.org/10.1016/j.neurobiolaging.2012.03.001.
[80] N.B. Hastings, X.H. Wang, L.X. Song, B.D. Butts, D. Grotz, R. Hargreaves, J.F. Hess, K.L.K. Hong, C.R.R. Huang, L. Hyde, M. Laverty, J.L. Lee, D. Levitan, S.X. Lu, M. Maguire, V. Mahadomrongkul, E.J. McEachern, X.S. Ouyang, T.W. Rosahl, H. Selnick, M. Stanton, G. Terracina, D.J. Vocadlo, G.F. Wang, J.L. Duffy, E. M. Parker, L.L. Zhang, Inhibition of O-GlcNAcase leads to elevation of O-GlcNAc tau and reduction of tauopathy and cerebrospinal fluid tau in rTg4510 mice, Mol. Neurodegener. 12 (2017), https://doi.org/10.1186/s13024-017-0181-0.
[81] M. Perluigi, E. Barone, F. Di Domenico, D.A. Butterfield, Aberrant protein phosphorylation in Alzheimer disease brain disturbs pro-survival and cell death pathways, Biochim. Biophys. Acta 1862 (10) (2016) 1871–1882, https://doi.org/10.1016/j.bbadis.2016.07.005.
[82] G. Bourre, F.X. Cantrelle, A. Kamah, B. Chambraud, I. Landrieu, C. Smet-Nocca, Direct crosstalk between O-GlcNAcylation and phosphorylation of tau protein investigated by NMR spectroscopy, Front. Endocrinol. 9 (2018) 595, https://doi.org/10.3389/fendo.2018.00595.
[83] S.A. Yuzwa, X. Shan, M.S. Macauley, T. Clark, Y. Skorobogatko, K. Vosseller, D. J. Vocadlo, Increasing O-GlcNAc slows neurodegeneration and stabilizes tau against aggregation, Nat. Chem. Biol. 8 (4) (2012) 393–399, https://doi.org/10.1038/nchembio.797.